Columnar growth in oblique incidence ballistic deposition: Faceting, noise reduction, and mean-field theory

Joachim Krug*

Theoretische Physik, Ludwig Maximilians Universität, Theresienstrasse 37, D-8000 München 2, Germany

Paul Meakin

*Central Research and Development Department, E. I. du Pont de Nemours and Company,
Experimental Station E356/153, Wilmington, Delaware 19880-0356*
(Received 13 August 1990)

Several aspects of the columnar structure encountered in vapor deposition at oblique particle incidence are studied through a combination of theoretical analysis and computer simulations. First, a general macroscopic theory of columnar growth is presented that yields, among other results, an expression for the columnar growth angle. We then focus on the role of noise in columnar growth, using two simple square-lattice ballistic deposition models—finite-density deposition and noise-reduced deposition—in which the amount of fluctuations in the growth process can be tuned by varying a control parameter. In both models faceting of the column tips stabilizes the columnar morphology. In the finite-density model, we find a faceting transition related to directed percolation. Some characteristics of columnar growth are retrieved within a mean-field approximation. Simulations carried out on d-dimensional hypercubic lattices up to $d = 6$ indicate that the deposit density converges to its mean-field value in the limit $d \to \infty$.

I. INTRODUCTION

Random fluctuations play an important part in most pattern-formation processes,[1] both at the onset of the instability[2] and during later stages such as dendritic side-branching[3] and coarsening.[4] The present paper addresses the role of fluctuations in the context of columnar growth, which is a ubiquitous phenomenon occurring in a variety of vapor-deposition processes.[5]

The basic mechanism that leads to unstable growth is easily accounted for.[5,6] Fluctuations in the deposition flux cause parts of the deposit to grow ahead of others. Under conditions of oblique particle incidence the protruding parts shadow the retarded ones, which consequently stop growing.[7] In the absence of surface diffusion[8,9] the most unstable wavelength is of the order of the particle size.[5]

Once columns have formed as a result of amplification of microscopic fluctuations, they continue to compete for the incoming flux through the very same mechanism, larger columns shadowing smaller ones and thus preventing them from further growth. Since the range of the shadowing interaction is not restricted by any additional length scale (such as, e.g., the diffusion length in dendritic growth[4]), this coarsening process continues indefinitely, leading eventually to a structure that is statistically scale invariant from the microscopic to the macroscopic scale.[10,11] Column formation is a consequence of a *competitive* growth process similar to (though better understood than) diffusion-limited deposition in the limit of zero particle density, corresponding to the diffusion length becoming infinite.[12] For two-dimensional deposition onto a line[10] the column spacing increases with the

deposit thickness h as $h^{1/2}$ and the column mass distribution has a power-law decay with an exponent $\tau = 4/3$. In three dimensions the columns form sheets that extend perpendicular to the deposition plane.[11] Their spacing grows as $h^{1/3}$ and the mass-distribution exponent takes the value $\tau = \frac{3}{2}$.

In our previous analysis[10,11] we focused on the limit of near grazing particle incidence, where the columns can be assumed to grow independently apart from the shadowing interaction. This assumption breaks down at intermediate angles of incidence, leading to a complex crossover behavior.[10] Numerically, a very gradual transition is observed[10,11,13] from the homogeneous porous structure that forms at normal particle incidence, to columnar growth, making it impossible to pin down a "phase" boundary between the two distinct growth morphologies. Here we attempt to clarify this point by investigating an extension[14] of the ballistic deposition model[15,16] used in our earlier work.[10,11,13]

Let us define then the models of interest. We consider a two-dimensional square lattice, the sites of which are either vacant or occupied by a deposit particle. A row of occupied sites parallel to the x axis constitutes the substrate. Next a particle is dropped above a randomly chosen substrate site x. The particle falls down vertically until it reaches a growth site, i.e., a vacant lattice site which is the nearest neighbor of an occupied (deposit or substrate) site. There the particle sticks and becomes part of the deposit. Denoting by $h_x(N)$ the maximum y coordinate of any occupied site above the substrate site x after deposition of N particles, the deposition event may be written as

$$h_x(N+1) = \max[h_{x+1}(N), h_x(N)+1, h_{x-1}(N)] . \quad (1.1)$$

Deposition at oblique particle incidence is modeled by choosing an inclined substrate as initial condition,

$$h_x(0) = [x \tan\theta] \,, \tag{1.2}$$

where θ is the angle formed by the particle trajectories with the substrate normal, and $[a]$ denotes the integer closest to a. We use helical boundary conditions in the lateral direction,

$$h_{x+L} = h_x + [L \tan\theta] \,, \tag{1.3}$$

where L is the lateral system size (note that the substrate length is $L/\cos\theta$). For the simulations described in this

paper we chose the system size $L = 2^{18} = 262\,144$ lattice spacings. The deposits typically contained $(1-2) \times 10^9$ particles.

From the point of view of applications we would like to know how the deposit structure depends on deposition conditions such as the substrate temperature and the rate of deposition.[17] The latter effect can be crudely incorporated in our simple lattice model by replacing the sequential updating (1.1) by a synchronous rule in which a *finite* fraction p, $0 < p < 1$, of all growth sites are updated *simultaneously*.[14] Time proceeds in discrete steps, $t = 0, 1, 2, \ldots$, and in one time step, $t \to t+1$, the surface configuration $h_x(t)$ evolves according to

$$h_x(t+1) = \begin{cases} \max[h_{x+1}(t), h_x(t)+1, h_{x-1}(t)] & \text{with probability } p \\ h_x(t) & \text{with probability } 1-p \,. \end{cases} \tag{1.4}$$

The parameter p controls the rate of deposition. In the "dilute" limit $p \to 0$ we recover the sequential rule (1.1).

In the context of the present work our interest in the finite deposition density model (1.4) derives from the fact that the parameter p allows us to tune the amount of noise in the growth process. To see this, we note that for $p = 1$ the growth rule (1.4) becomes deterministic. A caricature of columnar growth survives in the deterministic limit.[10] In particular, for $p = 1$ there is a *sharp* transition from layerwise to columnar growth at a critical angle $\theta_c = 45°$. Quite surprisingly, we find that the transition *remains* sharp for infinite noise strength, in a range $p_c < p < 1$, where p_c is the directed site percolation threshold.[18] In Sec. III we relate this behavior to a faceting transition of a type familiar from other synchronous growth models.[19−21] For $p > p_c$ and $\theta > \theta_c$ the columns have faceted tips. Our simulations show that this leads to scaling properties that are *independent* of the angle of incidence for $\theta > \theta_c$, and that conform to the predictions of our analysis[10] for independently growing columns. This indirectly demonstrates that the observed[10,13] continuous variation of scaling properties with θ in the model (1.1) can be attributed to fluctuations in the structure of the column tips that are absent in the faceted phase $(p > p_c)$ of the finite-density model (1.4). Faceted columnar growth has recently been found in molecular-dynamics simulations of the epitaxial growth of silicon.[22] We wish to stress, however, that the faceting transition investigated here is due to the (somewhat unrealistic) synchronous updating rule and does not have a clear physical interpretation. Still, our general conclusions concerning the influence of the tip fluctuations (or edge fluctuations in three dimensions[11]) upon the columnar structure are expected to carry over to real systems.

A different type of noise reduction has recently been applied to a variety of growth models.[23−26] In this algorithm, "counters" are placed on the growth sites, and a site is filled only after it has been randomly chosen a prescribed number of times, m. In some cases the limit $m \to \infty$ leads to a deterministic growth model.[27] For noise-reduced oblique-incidence ballistic deposition[13] it turns out that the growth rule retains some randomness even in the limit $m \to \infty$. We study the limiting model in

Sec. IV and show that it behaves quite similarly to the finite-density model (1.4) in the faceted phase. However, as has been pointed out in the context of the Eden model,[24] facets appear only at $m = \infty$. There is no faceting transition at finite m. Consequently, noise reduction with finite m is not expected[25,26] to change the large-scale statistical properties of a growth model except for an overall rescaling of time. In Ref. 13 no significant dependence of the deposit scaling properties on m was found. A third way of approaching the deterministic limit employs deposition on finite (narrow) strips with periodic boundary conditions, thus reducing selectively the long-wavelength components of the noise.[10] Obviously, the large-scale properties are trivial in this case.

Neglecting fluctuations altogether yields a mean-field description of the growth process.[28] A nonlinear evolution equation for the average density profile is derived, which has traveling wave solutions[29,30] corresponding to a uniformly growing deposit. In Sec. V we extend a previous mean-field treatment of ballistic deposition[31] to include oblique particle incidence and synchronous updating [Eq. (1.4)]. We compute the θ-p phase diagram, deposit densities, growth angles, and other properties. As the mean-field theory is expected[28,31] to become increasingly accurate in higher dimensions, we carry out large-scale simulations on d-dimensional hypercubic lattices up to $d = 6$. Average properties such as the deposit density are indeed found to approach their mean-field values (albeit slowly) for large d. However, the most characteristic features of the columnar structure are not reproduced by the mean-field approach, thus revealing the importance of a finite amount of fluctuations to initiate and actually stabilize this growth morphology.

As a prerequisite for the detailed discussion of specific deposition models, the following section reviews some general (model independent) macroscopic features[10,28] of columnar deposits.

II. MACROSCOPIC THEORY OF COLUMNAR GROWTH

Looking at a picture of a (real or simulated) columnar deposit, e.g., that shown in Fig. 1, several obvious ques-

tions concerning the macroscopic structure arise. We would like to know how (i) the *deposit density* and (ii) the *column orientation* depend on the angle of incidence, and (iii) what determines the *shape of clusters* grown by unidirectional deposition onto a point seed[32,33] (see Fig. 2). Here we show that the answers to all three questions are simply related to a single quantity, the *inclination-dependent growth velocity*.[28,34]

On a sufficiently coarse-grained level (coarser than the typical column width) the upper, accessible deposit surface can be described by a single-valued height function. To simplify notation we consider two-dimensional deposits on a one-dimensional substrate. The surface height at time t, $h(x,t)$, is measured in the direction of the incoming flux. The basic assumption of the theory is that the local growth velocity $v = \partial h/\partial t$ is determined by the local surface inclination $u = \partial h/\partial x$ through a function $v(u)$, the inclination-dependent growth velocity, which
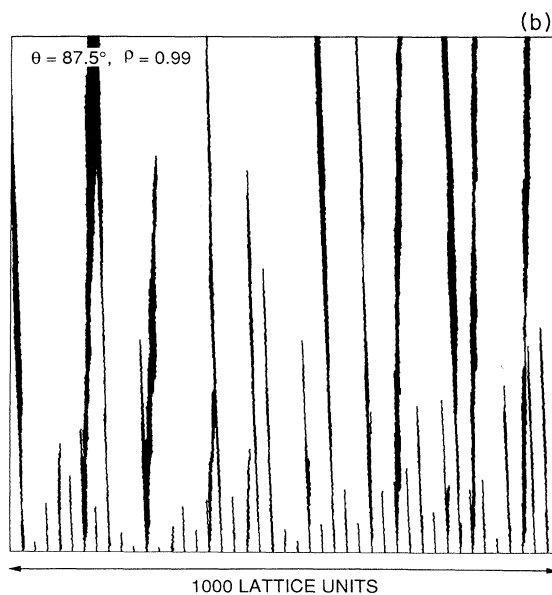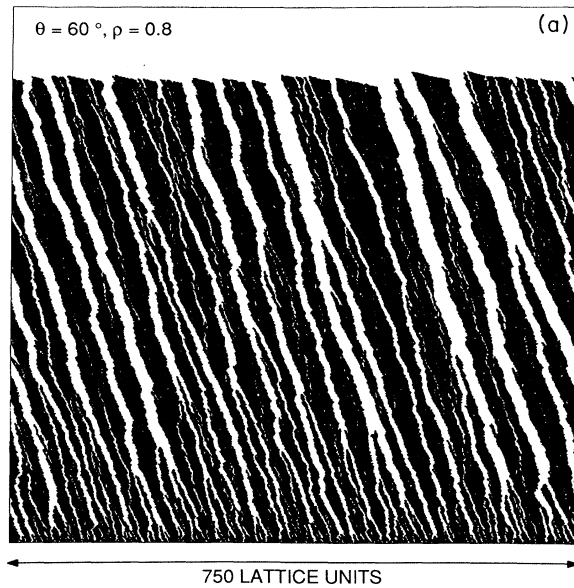

FIG. 1. Deposits generated using the finite-density ballistic deposition model on a square lattice. (a) Angle of particle incidence $\theta = 60°$, deposition flux parameter $p = 0.9$. (b) $\theta = 87.5°$, $p = 0.99$.
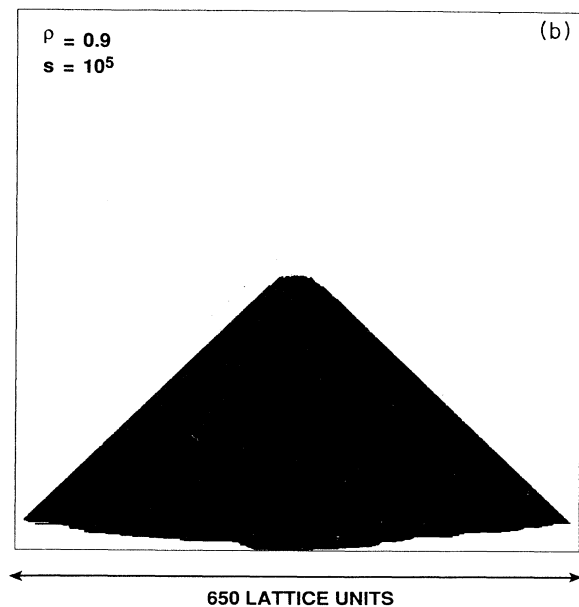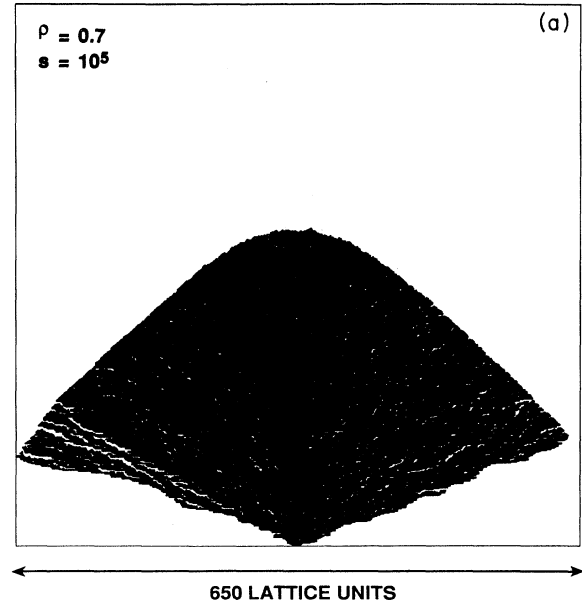
FIG. 2. Clusters generated by ballistic deposition onto a point seed, using the finite-density model on a square lattice. Each cluster contains 10^5 particles. (a) Deposition flux parameter $p = 0.7$. (b) $p = 0.9$.

contains the macroscopic information about the growth process. The equation of motion for $h(x,t)$ is then

$$\frac{\partial}{\partial t}h(x,t)=v\left[\frac{\partial}{\partial x}h(x,t)\right] . \tag{2.1}$$

In principle the function $v(u)$ can be derived, using the methods of statistical mechanics, from the underlying microscopic model. Empirically, it is obtained by measuring the velocity of a surface with *global* inclination u. For deposition processes the simple relationship[34]

$$v(u)=J/\rho(u) \tag{2.2}$$

follows from mass conservation. Here J is the deposition flux and $\rho(u)$ is the density of a deposit grown at inclination u, equivalently at an angle of incidence of $\theta=\arctan u$. Oblique incidence deposition generally leads to an increase in the porosity of the deposit, and hence $\rho(u)$ is a decreasing function of u.[17,35] In the following we shall therefore assume that $v(u)$ is a convex function, $v''(u)>0$, excluding cases[28,34,36] where $v(u)$ is a constant or shows a more complicated u dependence.

The local inclination $u(x,t)=(\partial/\partial x)h(x,t)$ evolves under (2.1) as

$$\frac{\partial}{\partial t}u(x,t)=v'(u(x,t))\frac{\partial}{\partial x}u(x,t) . \tag{2.3}$$

A piece of slope u translates along the x axis at velocity $-v'(u)$. After a short time dt its x coordinate has changed by $dx=-v'(u)dt$ and its h coordinate by $dh=[v(u)-uv'(u)]dt$. Hence the local direction of growth is given by the angle

$$\psi(u)=\arctan\{[v(u)/v'(u)-u]^{-1}\} \tag{2.4}$$

relative to the h axis. For columnar growth, it is very natural to identify $\psi(u)$ with the column orientation at an angle of incidence of $\theta=\arctan u$. Through (2.2) we have then related the angular variation of the columnar orientation to that of the deposit density.

Let us illustrate Eq. (2.4) by some simple examples. For isotropic growth at normal velocity $\hat{v}$, the inclination dependent growth velocity is $v(u)=\hat{v}(1+u^2)^{1/2}$. Inserting this into (2.4) we find $\psi=\theta$, as expected. We have shown previously[10] that columnar growth leads to a linear behavior of $v(u)$ at large u,

$$v(u)\approx v_{\perp}(u+a), \quad u\to\infty , \tag{2.5}$$

with positive constants $v_{\perp}$ and a. It then follows from (2.4) that[10]

$$\lim_{u\to\infty}\psi(u)=\psi_0=\arctan(1/a) . \tag{2.6}$$

Including a correction term in (2.5),

$$v(u)-v_{\perp}(u+a)\sim u^{-n} \tag{2.7}$$

for some $n>0$, we obtain to leading order

$$\psi_0-\psi\sim\left[\frac{\pi}{2}-\theta\right]^n \tag{2.8}$$

at near grazing incidence. The numerical results of Ref.

13 indicate that $\psi(u)$ approaches its limit with zero slope at $\theta=\pi/2$ (90°), i.e., $n>1$. For small u we expect $v(u)$ to be quadratic in u, $v(u)\approx v_0+(\lambda/2)u^2$. This yields a linear increase of the growth angle for small θ,

$$\psi\approx\frac{\lambda}{v_0}\theta , \tag{2.9}$$

as has been observed numerically.[13] In general, convexity of $v(u)$ implies that ψ is a monotonously increasing function of u, $\psi'(u)>0$. The famous "tangent rule"[5,37,33] $\tan(\theta-\psi)=\frac{1}{2}\tan(\theta)$ corresponds to the growth velocity $v(u)=v_0(1+u^2)^{1/4}$, which violates the convexity condition [note that multiplying $v(u)$ by a constant does not change $\psi(u)$]. Indeed, the tangent rule was recently refuted on the basis of extensive large-scale simulations.[13,16]

Ballistic deposition onto a point seed produces fan-shaped clusters[32,33] (see Fig. 2). For large clusters the upper cluster surface attains the scaling form

$$h(x,t)=t\mu(x/t) , \tag{2.10}$$

where the shape function μ is the Legendre transform of the growth velocity[10,28,38]

$$\mu(y)=\min_{u}[v(u)+uy] . \tag{2.11}$$

The linear asymptotics (2.5) of $v(u)$ maps onto the edges of the fan. The width of the fan is $2v_{\perp}t$ at time t, and its opening angle is $2\psi_0$, as would be intuitively expected. Hence the shape function $\mu(y)$ is defined for $-v_{\perp}\leq y\leq v_{\perp}$ and $\mu(\pm v_{\perp})=v_{\perp}/\tan\psi_0$. The behavior near the edges is related to the corrections to (2.5). For a correction term $O(u^{-n})$ [Eq. (2.7)] we find

$$\mu(y)-\mu(v_{\perp})\sim(v_{\perp}\mp y)^{n/(n+1)} \tag{2.12}$$

close to $y=\pm v_{\perp}$. The cluster surface joins the edges at infinite inclination, $\mu'(v_{\perp})=\infty$.

Another point of interest is the internal density distribution of the cluster.[32] It is convenient to introduce polar coordinates (r,ϕ), where the angle ϕ is measured relative to the vertical. The upper cluster surface is then described by a function $r(\phi)$, which is related to $\mu(y)$ through

$$\mu(y)=r(\phi)\cos\phi, \quad y=r(\phi)\sin\phi . \tag{2.13}$$

Let $\rho(\phi)$ denote the radially averaged density at a fixed angle ϕ. In the limit of infinite cluster size, $\rho(\phi)=0$ for ϕ outside the opening angle $\pm\psi_0$ of the fan. Obvious geometric considerations show that $\rho(\phi)$ is still given by the simple expression (2.2), if the local slope $\mu'(y)$ of the cluster surface is substituted for u. The asymptotics (2.5) then implies that $\rho(\phi)\sim 1/\mu'(y)$ close to the edges. From (2.12) we infer that $\mu'(y)$ diverges as $(v_{\perp}-y)^{-1/(n+1)}$ for $y\to v_{\perp}$, and using (2.13) this translates into

$$\rho(\phi)\sim(\psi_0-|\phi|)^{1/n} \tag{2.14}$$

for $\phi\to\pm\psi_0$. Such power-law behavior has been observed numerically in simulations of both on- and off-lattice ballistic deposition.[32] Using a finite-size scaling ansatz,

Liang and Kadanoff estimate $1/n \simeq 0.23$ for the on-lattice case, while Joag et al. obtain $1/n \simeq 0.33$ from off-lattice simulations. This is consistent with our previous conclusion that $n > 1$ in these models. As the definition (2.7) suggests an integer value for n, the numerical estimates could be taken to indicate that $n = 3$ or 4. We are not aware of any argument as to why n should be universal (model independent), quite in contrast to the power-law finite-size corrections also studied in Ref. 32, which can be related[39] to the universality of kinetic roughening.[28]

Summarizing, we have shown that the three basic macroscopic quantities—the deposit density ρ, the column orientation ψ, and the cluster shape μ—contain equivalent information, which can be extracted from any one of them using simple transformations. In that sense, they are analogous to the thermodynamic potentials for equilibrium systems. In fact, the analogy to thermodynamics[40] also extends to morphological transitions, which show up as singularities in the "potentials" ρ, ψ, and μ. One example is the occurrence of linear pieces in the inclination-dependent growth velocity [Eq. (2.5)], which reflects the growth of independent, well-separated columns (cf. Ref. 10 and Sec. III below.) Another example of relevance here is a break in the slope of $v(u)$ at some u_0,

$$v(u) \approx v(u_0) + b(u - u_0) + c|u - u_0| . \tag{2.15}$$

This leads to a jump in the column orientation, and a facet of size $2c$ in the scaled cluster shape.

III. THE FACETING TRANSITION

A. Macroscopic features

In the deterministic limit $p = 1$ of the rule (1.4), growth proceeds in compact layers for inclinations $u \leq 1$, while for $u > 1$ void formation through shadowing leads to a deposit density $\rho(u) < 1$. The inclination-dependent growth velocity is[10]

$$v(u) = \begin{cases} 1, & u \leq 1 \\ u, & u > 1 , \end{cases} \tag{3.1}$$

with a break in slope at $u = 1$. Accordingly, the growth shape is a fully faceted triangle, from Eq. (2.11)

$$\mu(y) = 1 - |y|, \quad -1 \leq y \leq 1 . \tag{3.2}$$

In Fig. 3(a) we show the numerically determined inclination-dependent growth velocity for various values of $p < 1$. Here time is counted as the number of applications of the synchronous growth rule (1.4). Since in each time step a fraction p of all growth sites is filled, the particle flux in Eq. (2.2) is $J = p$, and the deposit density is $\rho(u) = p/v(u)$. Clearly for fixed u, $v(u)$ has to be an increasing function of p. The remarkable feature about the data presented in Fig. 3(a) is that at $u = 1$ ($\theta = 45°$) the growth velocity sticks to its maximum ($p = 1$) value $v = 1$, and the break in slope present for $p = 1$ persists, for large enough p.

The reason for this behavior is the existence of a directed percolation process[18] embedded in the growth pro-

cess.[19] Consider a substrate inclined at $u = 1$, $h_x = x$ at $t = 0$. Then at time t the deposit cannot extend beyond the line

$$\Lambda_t = \{(x,y) \in \mathbb{Z}^2 | y - x = t \} . \tag{3.3}$$

Let B_t denote the set of occupied sites on that line. This set has an autonomous time evolution; i.e., B_t depends only on B_{t-1}. A site $(x,y) \in \Lambda_t$ belongs to B_t with probability p, if at least one of its two neighbors $(x + 1, y)$ and $(x, y - 1)$ belongs to B_{t-1}. This defines a one-dimensional contact process equivalent to directed site percolation.[18] There is a percolation threshold p_c (with $p_c \simeq 0.705\,489$ on the square lattice[18]) such that for $p < p_c$ the set B_t is empty for large t, while for $p > p_c$ it always contains a
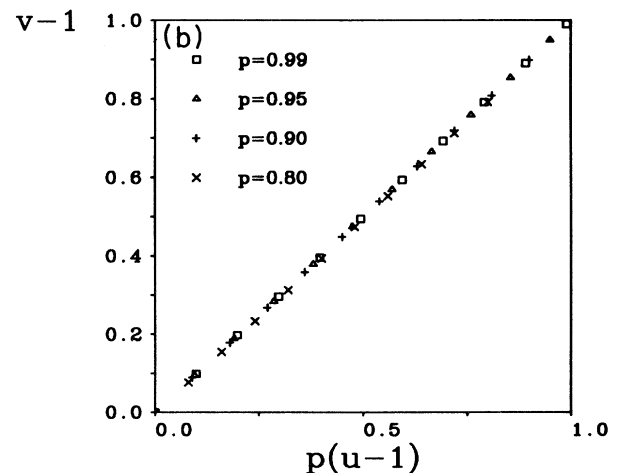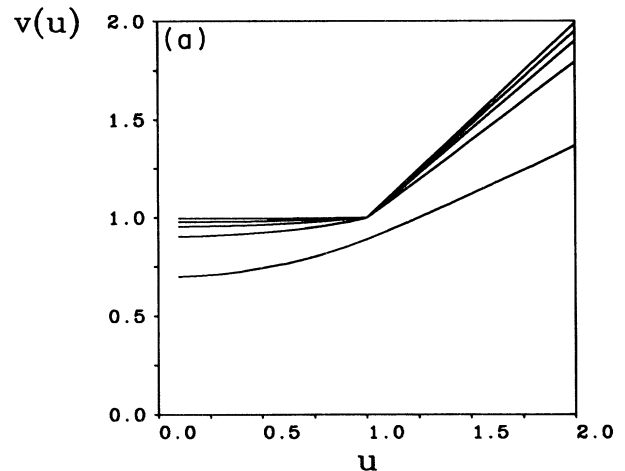

FIG. 3. Inclination-dependent growth velocity $v(u)$ for the finite-density model. (a) The values of the flux parameter p for the different curves are, from top to bottom, $p = 0.99$, 0.95, 0.9, 0.8, and 0.5. Simulations were carried out on a substrate of width $L = 1000$, and 5000 time steps were performed for each value of u and p. (b) The data for $p > p_c$ and $u > 1$ rescaled according to (3.15).

finite fraction of the sites in Λ_t. Specifically, the density $\sigma(t)$ of occupied sites in Λ_t decays exponentially for $p < p_c$, $\sigma(t) \sim e^{-t/\xi_t}$, with a relaxation time ξ_t diverging as

$$\xi_t \sim (p_c - p)^{-\nu_t} \qquad (3.4)$$

for $p \to p_c$ from *below*. For $p > p_c$, $\sigma(t)$ has a finite limit $\sigma_0 = \lim_{t \to \infty} \sigma(t) > 0$, which vanishes as

$$\sigma_0 \sim (p - p_c)^{\beta_{DP}} \qquad (3.5)$$

for $p \to p_c$ from *above*. At the critical point $p = p_c$ the decay of $\sigma(t)$ is algebraic,

$$\sigma(t) \sim t^{-\beta_{DP}/\nu_t} \quad . \qquad (3.6)$$

Here ν_t and β_{DP} are critical exponents which govern the behavior of the "order parameter" σ close to the transition. In two dimensions[18] $\nu_t \simeq 1.733$ and $\beta_{DP} \simeq 0.277$.

Now the transition in $v(u)$ can be easily understood. For $p > p_c$ the deposit surface sticks to the line Λ_t and $v(1) = 1$, whereas for $p < p_c$ it loses contact and $v(1) < 1$. To describe the behavior below p_c Kertész and Wolf[20] introduced the subcritical order parameter $V = 1 - v(1)$ and showed that

$$V \sim \xi_t^{-1} \sim (p_c - p)^{\nu_t} \qquad (3.7)$$

for $p \to p_c -$. At the critical point V decays as

$$V \sim 1/t \quad . \qquad (3.8)$$

Using the relation (2.2) with $J = p$ this implies that the deposit density at 45° ($u = 1$) is

$$\rho(1) = p \qquad (3.9)$$

for $p > p_c$. At p_c there is a weak singularity in $\rho(1)$,

$$\rho(1) - p \sim (p_c - p)^{\nu_t} \qquad (3.10)$$

for $p \to p_c -$, in accordance with the numerical results shown in Fig. 4.

The discussion of inclination-dependent properties requires introducing one further critical exponent. Suppose we start the directed percolation process from a single seed site ($B_0 = \{0,0\}$) rather than from a line of filled sites. During its lifetime ξ_t (for $p < p_c$) the set B_t then reaches a typical width ξ_r which diverges as

$$\xi_r \sim (p - p_c)^{-\nu_r} \qquad (3.11)$$

for $p \to p_c -$, with $\nu_r < \nu_t$ and $\nu_r \simeq 1.097$ in two dimensions.[18] The critical behavior of $v(u)$ can be expressed[21] in terms of ν_t and ν_r. In particular, for $p > p_c$ there is a break in slope at $u = 1$, cf. Eq. (2.15), of magnitude

$$c \sim (p - p_c)^{\nu_t - \nu_r} \qquad (3.12)$$

for $p \to p_c +$. At criticality ($p = p_c$) the singularity is weaker,

$$v(u) \approx 1 + b'(u - 1) + c'|u - 1|^{\nu_t/\nu_r} \qquad (3.13)$$

close to $u = 1$, with positive constants b', c'. The expression (2.4) for the columnar growth angle then yields a
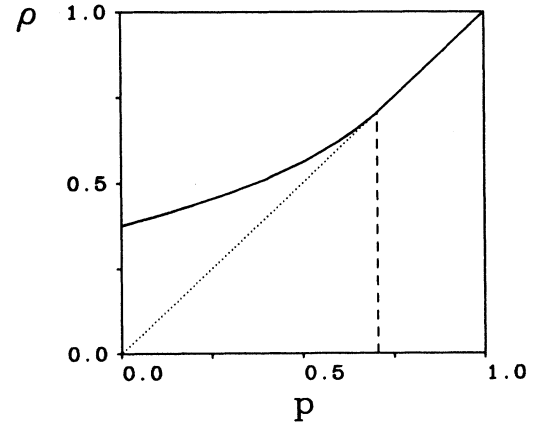

FIG. 4. Simulation results for the deposit density ρ as a function of the deposition flux p at an angle of incidence $\theta = 45°$. The dotted line indicates the behavior $\rho = p$ expected in the faceted phase $p > p_c$, and the dashed line shows the position of p_c.

discontinuity in $\psi(u)$ at $u = 1$ and $p > p_c$ of a magnitude proportional to c, and a singularity

$$\psi(u) - \psi(1) \sim \mp |u - 1|^{\nu_t/\nu_r - 1} \qquad (3.14)$$

at p_c, where the $-$ (+) sign refers to $u < 1$ ($u > 1$). Note that, since $\nu_t/\nu_r < 2$, Eq. (3.14) implies an infinite derivative of $\psi(u)$ at p_c. This is qualitatively confirmed by the simulation results for the growth angle[41] presented in Fig. 5, although the exponent in (3.14) could not be extracted from the data.
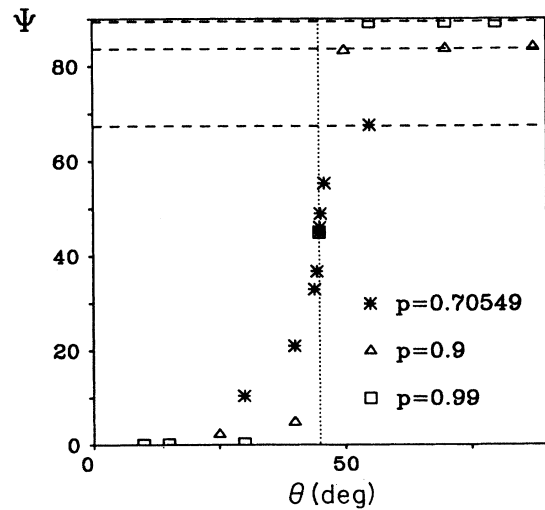

FIG. 5. Simulation results for the column orientation ψ as a function of the angle of incidence θ for various values of the flux p. The dotted line indicates the critical angle $\theta_c = 45°$ where the column orientation is expected to jump for $p > p_c$. The dashed lines show the prediction (3.16) for $\theta > \theta_c$.

Upon closer inspection the data depicted in Fig. 3 reveal that $v(u)$ is *strictly* linear in u for $u > 1$ and $p > p_c$. We noted already that this is to be expected for *large u*, cf. Eq. (2.5). The asymptotic slope $v_\perp$ is easily determined for the model (1.4). Consider for this purpose the growth of a fan from a point seed, as shown in Fig. 2. At each time step the leftmost and the rightmost growth site of the fan have a probability of p each to become filled. Hence the fan widens at the rate $2p$ and $v_\perp = p$, leading to the asymptotic behavior $v(u) \approx p(u + a)$ for the growth velocity. The simulation results in the faceted phase $(p > p_c)$ indicate that this behavior extends all the way to $u = 1$. Since $v(1) = 1$ in the faceted phase, this also fixes the constant a in (2.5), whence

$$v(u) = 1 + p(u - 1) , \qquad (3.15)$$

cf. Fig. 3(b). The theory of Sec. II then predicts that the columnar growth angle $\psi(u)$ is constant for $u > 1$, $\psi(u) \equiv \psi_0$ with

$$\psi_0(p) = \arctan\left[\frac{p}{1-p}\right] , \qquad (3.16)$$

in agreement with the numerical data shown in Fig. 5.

Hence for $p > p_c$ the finite-density model (1.4) shows the macroscopic characteristics[10] of columnar structure—a linear growth velocity $v(u)$ and a constant growth angle $\psi(u)$—for all inclinations $u > 1$, indicating a sharp onset of "ideal" columnar growth at $\theta = 45°$. Below we shall reach the same conclusion regarding the scaling properties of the deposit. The picture of well-separated columns growing independently (except for the shadowing) is supported by the visual appearance of the deposits, cf. Fig. 1. The figure also gives a clue to what we believe to be the mechanism behind this behavior, namely the *faceted tips* of the columns. We noted already that a break in the slope of $v(u)$ leads, through the Legendre transform (2.11), to a facet in the corresponding cluster shape. Here the fact that $v(u)$ is linear for all $u > 1$ implies that the facets extend to the very edges of the cluster, as can be seen in Fig. 2. It is rather obvious that a column, provided it survives, grows in the same manner as the outermost edges of the fan, and thus its exposed part is expected to be faceted for all $p > p_c$. This is what distinguishes the columnar structure above p_c from that below p_c, where both $v(u)$ and $\psi(u)$ vary smoothly (nonlinearly) with u. We note that these arguments do not really *explain* the occurrence of ideal columnar growth above p_c, since the linearity of $v(u)$ in turn arises from the structure itself. Still we feel that a rather satisfying understanding has been reached in terms of the general notions of Sec. II.

B. Kinetic roughening

The fluctuations of the upper deposit surface are described by the root-mean-square (rms) roughness $\xi(t)$, which is defined by

$$\xi(t)^2 = \frac{1}{L} \sum_{x=1}^{L} [h_x(t) - h_x(0) - \bar{h}(t)]^2 , \qquad (3.17)$$

where

$$\bar{h}(t) = \frac{1}{L} \sum_{x=1}^{L} [h_x(t) - h_x(0)] \qquad (3.18)$$

denotes the average deposit thickness. In the limit of large system size $(L \to \infty)$, $\xi(t)$ has a power-law behavior,

$$\xi(t) \sim t^\beta . \qquad (3.19)$$

For a locally smooth, one-dimensional surface, the continuum theory of Kardar, Parisi, and Zhang[28,42] predicts that $\beta = \frac{1}{3}$ in generic cases.[34] A relevant example of this class of processes is ballistic deposition at *normal* particle incidence.[14-16] On the other hand, the limit of *near-grazing* incidence can be treated by a simplified model of independently growing columns which interact only through shadowing,[10] leading to the result $\beta = \frac{1}{2}$. It is then natural to ask how the exponent behaves between the two limiting cases. Large-scale simulations of various models[13,35] indicate a continuous change in β, the asymptotic behavior of $\xi(t)$ being consistent with neither $\beta = \frac{1}{3}$ nor with $\beta = \frac{1}{2}$ at intermediate angles of incidence.

For the finite-density model (1.4) we observe the same qualitative behavior *below* the faceting transition, $p < p_c$. However, in the faceted regime the situation is quite different (Fig. 6). As explained above, the embedded directed percolation process forces a surface growing at $\theta = 45°$ to stick to the line Λ_t if $p > p_c$. This constrains the surface fluctuations, and the roughness (3.17) tends to a finite limit of order unity, i.e., $\beta = 0$. Hence the rough "phases" for $\theta < 45°$ and $\theta > 45°$ are separated by a flat phase[43] at $\theta = 45°$. Extensive simulations at various an-
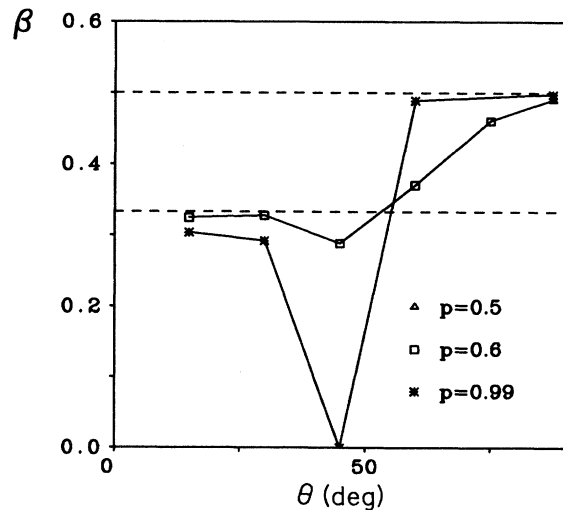

FIG. 6. Effective kinetic roughening exponent β as a function of the angle of incidence for $p < p_c$ (open symbols) and $p > p_c$ (solid symbols). The dashed lines indicate the theoretical predictions $\beta = \frac{1}{3}$ for continuous growth and $\beta = \frac{1}{2}$ for columnar growth.

gles and various values of p (an example is shown in Fig. 7) show that this leads to asymptotic exponents which are *independent* of θ both below 45°, where $\beta \simeq \frac{1}{3}$, and above 45°, where $\beta \simeq \frac{1}{2}$ (Fig. 6). As discussed already, we attribute this behavior to the faceting of the column tips for $p > p_c$. In the faceted phase, the tip fluctuations which destabilize the columnar structure[10] are suppressed, and our picture of ideal columnar growth[10] applies without reservations.

Close to $\theta = 45°$, the vicinity of the flat phase leads to a delay of the kinetic roughening process. The crossover scaling form follows from a simple mechanism which we describe here only for $\theta > 45°$. The case $\theta < 45°$ is quite analogous. Consider a substrate of inclination $u = \tan\theta = 1 + \epsilon$, $\epsilon \ll 1$. According to (1.2) the substrate consists of pieces of length ϵ^{-1} which have unit slope ("facets"), which are separated by double steps where $h_{x+1} - h_x = 2$. For $p > p_c$, each of the facets grows at unit velocity, remaining flat, except for the two sites at the facet boundaries. By inspection of the growth rule it is found that the facet boundaries perform random walks in the transverse direction. Due to shadowing, neighboring facets cannot coalesce, but facets can disappear if their two boundaries meet. This happens after a time of the order ϵ^{-2} and marks the onset of roughening. Thus we expect the scaling form

$$\xi(t) = f((u-1)^2 t) , \qquad (3.20)$$

where $f(x \to 0) = \text{const}$ and $f(x \to \infty) \sim x^{1/2}$. This form is well supported by the numerical data up to $\theta \simeq 47°$ (Fig. 8).

A different scaling form applies at the directed percolation threshold $p = p_c$. For p close to p_c, the facet size ϵ^{-1} should be compared to the transverse directed percolation length ξ_r, and the time t to the relaxation time ξ_t. Thus we expect the general form

$$\xi(t) = F((u-1)\xi_r, t/\xi_t) . \qquad (3.21)$$

Approaching p_c from above at fixed t and u, the arguments in (3.21) must combine such that the divergencies of ξ_r and ξ_t cancel. Using Eqs. (3.4) and (3.11), we conclude that

$$\xi(t) = \tilde{f}[(u-1)^{\nu_t/\nu_r} t] \qquad (3.22)$$

at $p = p_c$, where the scaling function $\tilde{f}$ has the same asymptotics as f in (3.20). Our simulation results presented in Fig. 9 confirm this form, with $\nu_t/\nu_r \simeq 1.58$ in two dimensions.[18]

It remains to consider the critical point $u = 1$, $p = p_c$, which is not covered by the scaling form (3.22). Integrating the critical decay law (3.8) for the order parameter $V = 1 - v(1)$, we see that the distance of the growing surface to the "causality" limit Λ_t increases as $\ln t$. Since the surface fluctuations have to fit into this gap, it follows[20] that $\beta = 0$ up to logarithms. Numerically, we find (Fig. 10)

$$\xi(t) \sim (\ln t)^{\tilde{\beta}} , \qquad (3.23)$$

with $\tilde{\beta} \simeq 0.4$. This is consistent with the value $\tilde{\beta} \simeq 0.5$ obtained by Kertész and Wolf[20] for a related model of crystal growth, indicating that the anomalous roughening exponent $\tilde{\beta}$ may be universal. No theory for determining $\tilde{\beta}$ is available yet.

C. Scaling properties of the columnar structure

The most striking feature of the deposits shown in Fig. 1 is their scale invariance: The competitive growth process generates columns in a range of sizes extending from the lattice constant to the deposit thickness. We may distinguish two kinds of scaling properties:[44,45]

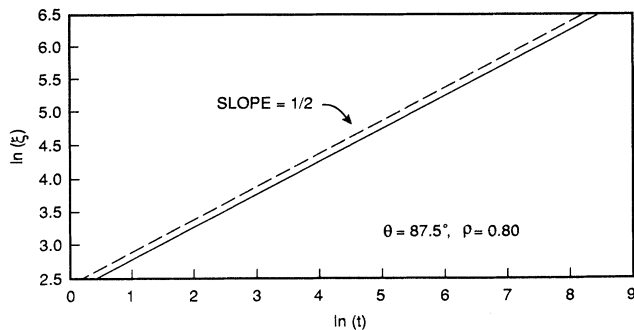FIG. 7. Surface roughness $\xi(t)$ at an angle of incidence $\theta = 87.5°$ and a deposition flux $p = 0.8$. A least-squares fit of the depicted data yields the estimate $\beta = 0.5026 \pm 0.0004$ for the kinetic roughening exponent.
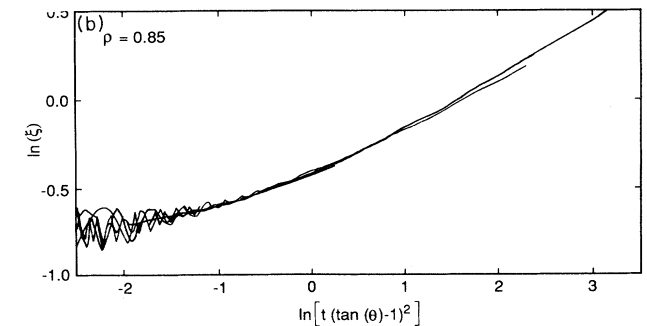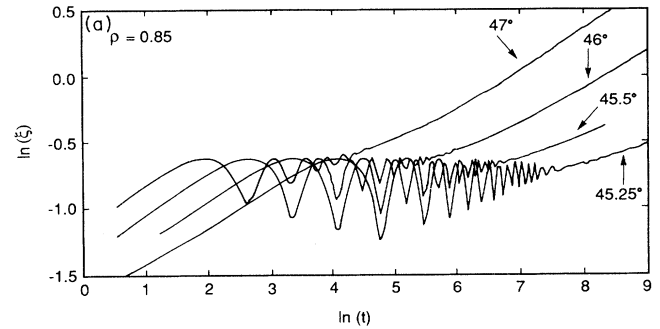
FIG. 8. Numerical verification of the scaling form (3.20) close to $u = 1$. (a) shows the surface roughness $\xi(t)$ for $p = 0.85$ and four different angles of incidence, and (b) shows the same data scaled according to (3.20).
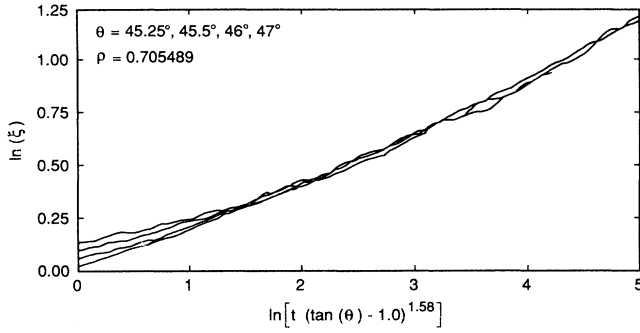
FIG. 9. Numerical verification of the scaling form (3.22) for the surface roughness close to $u=1$ at the directed percolation threshold $p=p_c \simeq 0.705\,489$.

(i) The deposit as a whole is characterized by a power-law size distribution; i.e., the number $n(s)$ of columns of mass s scales as

$$n(s) \sim s^{-\tau} . \tag{3.24}$$

(ii) The shape of individual columns is characterized by the scaling of their typical height, $h(s)$, and width, $w(s)$, with the mass s,

$$h(s) \sim s^{\nu_\parallel}, \quad w(s) \sim s^{\nu_\perp} . \tag{3.25}$$

Since $\nu_\parallel > \nu_\perp$, these structures are referred to as self-affine fractals.[45] Simplifications arise from the fact that both the deposit as a whole and the individual columns have a finite density. For a d-dimensional deposit, this implies the scaling relations[44,45]

$$\nu_\parallel + (d-1)\nu_\perp = 1 \tag{3.26}$$

and

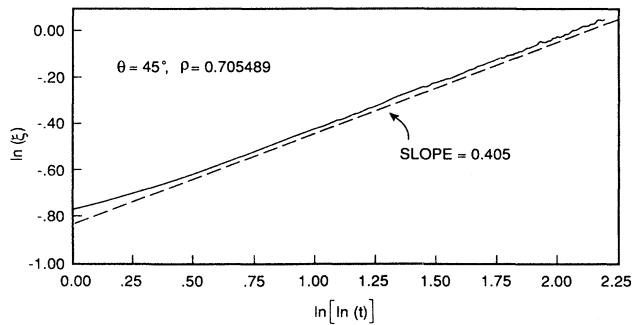$$\tau = 2 - \nu_\parallel , \tag{3.27}$$

leaving one exponent undetermined.

FIG. 10. Anomalous roughening at $\theta=45°$, $p=p_c$. The dashed line shows the logarithmic behavior $\xi(t) \sim (\ln t)^{0.4}$ of the surface roughness.

In our previous study we showed[10] that an array of well-separated columns which interact only through self-shadowing is characterized, in two dimensions, by the scaling exponents

$$\tau = \tfrac{4}{3}, \quad \nu_\parallel = \tfrac{2}{3}, \quad \nu_\perp = \tfrac{1}{3} . \tag{3.28}$$

In view of the results presented in the preceding sections, we expect the exponents (3.28) to apply in the whole faceted columnar phase $\theta > 45°$, $p > p_c$. This is confirmed by our extensive large-scale simulations (see Fig. 11 for an example). Below p_c the exponents show a similar continuous variation with the angle of incidence as was observed[13] for the sequential model (1.1), and the values (3.28) are approached only in the limit of near-grazing incidence.

Meakin[44] has pointed out that there is a natural decomposition of the deposit into "columnar" clusters even in cases when the deposit appears visually homogeneous. At the beginning of a simulation, the substrate sites are labeled by their coordinates. Then each newly deposited particle is given the same label as one (possibly randomly chosen) of the deposit or substrate sites to which it sticks. Deposit particles belong to one cluster if they share the same "ancestor" substrate site. For columnar growth, this definition of columns coincides with the obvious one. For ballistic deposition at normal
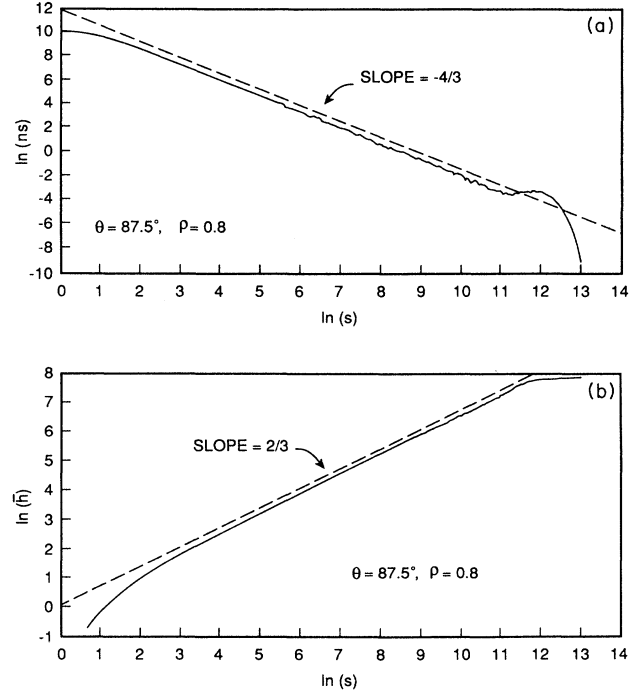

FIG. 11. Scaling of the columnar structure at $\theta=87.5°$ and $p=0.8$. (a) Number $n(s)$ of columns of mass s. A least-squares fit to the depicted data gives the estimate $\tau=1.332\pm0.004$ for the size-distribution exponent. (b) Average height $h(s)$ of columns of mass s. The depicted data yield the estimate $\nu_\parallel = 0.674\pm0.001$ for the substructure exponent.

incidence, we have shown[10] that the substructure exponents (3.25) are related to the dynamic surface exponent z, which describes the dynamic spreading of fluctuations parallel to the surface[10,28,42,46] through

$$v_\parallel / v_\perp = z \ . \tag{3.29}$$

In two dimensions[42] $z = \frac{3}{2}$, which yields, together with the relations (3.26) and (3.27), the scaling exponents[10,44]

$$\tau = \tfrac{7}{5}, \quad v_\parallel = \tfrac{3}{5}, \quad v_\perp = \tfrac{2}{5} \ . \tag{3.30}$$

Here we wish to address the behavior of the substructure exponents at $\theta = 45°$. As explained above, for $p > p_c$ the surface is flat at this angle, which separates the regions of continuous and columnar growth. In Fig. 12 we show estimates for the size-distribution exponent τ obtained from large-scale simulations at $\theta = 45°$ and various values of p. For small p, τ lies in the crossover regime[10,13] between the normal-incidence value $\tau = \tfrac{7}{5}$ and the near-grazing-incidence value $\tau = \tfrac{4}{3}$. Slightly below p_c the effective exponent rises toward the normal-incidence value and then drops rather abruptly to a value close to $\tfrac{4}{3}$ for $p > p_c$. At $p = p_c$ the dynamic surface exponent z can be shown[20] to be related to the directed percolation exponents through a relation analogous to (3.29), $z = v_t / v_r$. Combining this result with the scaling relations (3.26), (3.27), and (3.29), we obtain

$$\tau = \frac{v_t + 2(d-1)v_r}{v_t + (d-1)v_r}, \quad v_\parallel = \frac{v_t}{v_t + (d-1)v_r} ,$$
$$v_\perp = \frac{v_r}{v_t + (d-1)v_r} \ . \tag{3.31}$$

In two dimensions[18] this implies $\tau \simeq 1.388$, $v_\parallel \simeq 0.612$, which is consistent with the numerically determined
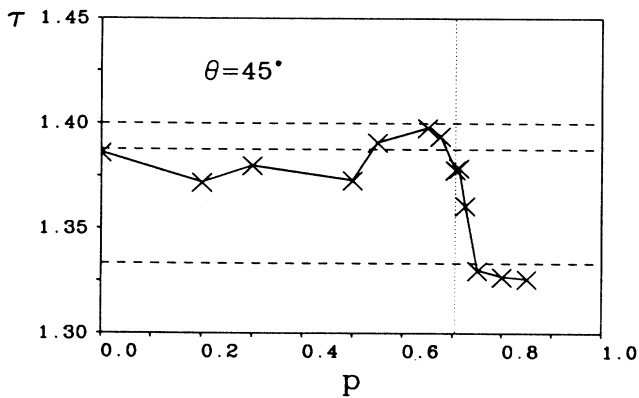

FIG. 12. Effective column size distribution exponent τ as a function of p at the critical angle of incidence $\theta = 45°$. The dashed lines indicate the values expected at normal incidence, $\tau = \tfrac{7}{5}$, at $p = p_c$, $\tau \simeq 1.388$, and at near-grazing incidence, $\tau = \tfrac{4}{3}$. The dotted line marks the transition point p_c. The statistical uncertainties are of the order of the symbol size. They were estimated by comparing the data to the exact scaling relation (3.27).

values $\tau = 1.378$, $v_\parallel = 0.623$ at $p = p_c$. However, it is clear from Fig. 12 that the statistical uncertainties in the measured exponents hardly allow us to resolve the tiny differences between the two sets of exponents (3.30) and (3.31).

To understand the behavior of τ for $p > p_c$, it is useful first to consider the seemingly trivial case $p = 1$. In each time step $t \rightarrow t+1$, the line Λ_{t+1} is completely filled. Every newly added particle has two neighbors on the line Λ_t. According to the procedure[44] described above, it is randomly connected to one of them. The array of clusters obtained in this way is identical to Scheidegger's random river network,[44,47] which is one of the simplest models for competitive growth. The individual clusters are the *critical* clusters of an exactly solved directed percolation model due to Domany and Kinzel.[48] In this model the starting configuration is a single filled site on the line Λ_0. Then subsequent configurations are generated using the following conditional probabilities: A site in Λ_{t+1} remains empty if both its backward neighbors in Λ_t are empty, it is filled if both neighbors are occupied, and it is filled with probability P if one of the neighbors is occupied. As a consequence, the boundaries of the cluster execute random walks in the transverse direction, which are biased inwards for $P < \tfrac{1}{2}$ and outwards for $P > \tfrac{1}{2}$. The Scheidegger model corresponds to the critical point $P = \tfrac{1}{2}$. The walks are then unbiased, and the scaling exponents are easily shown[47,48] to be given by Eq. (3.28). An alternative derivation which is valid in arbitrary dimension is sketched below.

For $p_c < p < 1$ the equivalence to the Scheidegger model is no longer complete, as holes appear in the set B_t of occupied sites at the maximum level Λ_t. Still, we know that B_t retains a finite density asymptotically. Hence the deposition events occurring in Λ_t can be thought to generate the backbone of the substructure pattern, which is expected to have the same scaling properties as the "undiluted" Scheidegger network. We conclude that the exponents (3.28) describe the whole faceted phase at $\theta = 45°$, in good agreement with the simulation results in Fig. 12. Note that the mechanism[10] leading to the same set of exponents (3.28) for $\theta > 45°$ is quite different, although in both cases coalescing random walks[49] enter the play.

The above arguments naturally extend to arbitrary dimension. We consider a d-dimensional hypercubic lattice with a surface growing perpendicular to the $(1,1,\ldots,1)$ direction. In the faceted phase, the surface sticks to the hyperplane $\Lambda_t^{(d)} = \{x_1 + x_2 + \ldots x_d = t\}$. In the corresponding d-dimensional Scheidegger model,[47] for simplicity at $p = 1$, each site in $\Lambda_{t+1}^{(d)}$ is connected to a randomly chosen neighbor in $\Lambda_t^{(d)}$ (there are d such neighbors). Consider a network grown to a height of h layers. We pick an arbitrary site in $\Lambda_h^{(d)}$ and follow its connections downward towards the substrate. Clearly, the path we follow is a random walk in the $d-1$ transverse directions. Occasionally the path coalesces with paths originating from other sites in $\Lambda_h^{(d)}$. Hence the number of root sites on the substrate which are connected to the top layer—equivalently, the number of clusters surviving up to height h—is proportional to the density $n(h)$ of a sys-

tem of *coalescing random walks* in $d-1$ dimensions, at time h. It can be proven[49] that $n(h) \sim h^{-1/2}$ for $d-1=1$, $n(h) \sim (\ln h)/h$ for $d-1=2$, and $n(h) \sim 1/h$ for $d-1 \geq 3$. The high-dimensionality result follows from the naive rate equation $dn/dh \sim -n^2$, which implies the "mean-field" assumption that the density of walkers is homogeneous in space. In that sense, $d=3$ is the upper critical dimension of the problem.[50] From the definitions (3.24) and (3.25) of the substructure exponents we infer that $n(h) \sim h^{-(\tau-1)/\nu_\parallel}$ in general. Thus for $d=2$ we recover the results (3.28). For $d \geq 3$ we conclude that $\tau - 1 = \nu_\parallel$, and using (3.27) we obtain

$$\tau = \tfrac{3}{2}, \quad \nu_\parallel = \tfrac{1}{2} \quad \text{for } d \geq 3 , \tag{3.32}$$

with logarithmic corrections in $d=3$. Since the walkers move diffusively, the linear size w of the region in $\Lambda_h^{(d)}$ that belongs to a single cluster is proportional to $h^{1/2}$. With (3.25) this implies $\nu_\parallel / \nu_\perp = 2$, and hence

$$\nu_\perp = \tfrac{1}{4} \quad \text{for } d \geq 3 . \tag{3.33}$$

The result (3.32) for τ is consistent with numerical simulations[47] of the Scheidegger model in dimensions $d = 3-6$. Note that the scaling relation (3.26) is satisfied by the exponents (3.32) and (3.33) only in the marginal dimension $d=3$. For $d > 3$ the individual clusters are no longer compact, but have a fractal dimension

$$D = \frac{d}{\nu_\parallel + (d-1)\nu_\perp} = \frac{4d}{d+1} . \tag{3.34}$$

IV. NOISE-REDUCED BALLISTIC DEPOSITION

In Ref. 13 two different noise-reduction algorithms[23,25] were applied to the basic square-lattice model (1.1). In model I a counter is associated with each growth site (x, g_x), where

$$g_x = \max(h_{x+1}, h_x + 1, h_{x-1}) . \tag{4.1}$$

The counter is increased by one each time the site is selected for deposition. After a preassigned number of selections m the site is filled and the counters corresponding to the newly created growth sites are set to zero. In model II the counters are associated with the substrate sites x instead. When deposition has been attempted m times above a given substrate site x, the *current* growth site (x, g_x) above x is filled and the counter is reset to zero. In this section we study the limiting case $m \to \infty$ of models I and II. In particular, we derive the exact inclination-dependent growth velocity for model I in that limit, and compare it to the results obtained for the finite-density model (1.4).

For the square-lattice model on a strip of width L there are L current growth sites at any time, one for each substrate site x, and therefore L counters. When m is large, the relative fluctuations in the counter positions become small. Consider an arbitrary counter which has just ripened,[25] i.e., its position has just passed the value m and it has been reset to zero. For large m it is almost certain that the other $L-1$ counters ripen before the

counter under consideration reaches m the next time. Hence in the limit $m \to \infty$ the counters ripen in *generations*, which we may choose as our unit of time. (We assume for the moment that all counters reach maturity, which is not true for model I, see below.) Within each generation the order in which the counters ripen is still random. The counter associated with the substrate site x is the kth one to ripen, where $k = \pi(x)$ and π is a randomly chosen permutation of the numbers $1, \ldots, L$. For normal-incidence deposition the order in which the sites ripen is clearly irrelevant, so growth proceeds layerwise and $v(0) = 1$ in our units of time. However, for a tilted substrate this is no longer true, as previous depositions at neighboring sites can shadow or shift the current growth site. A similar effect occurs in version C of the noise-reduced Eden model.[25]

Here an important difference arises between models I and II. For model II the counters are unaffected by previous deposition events at neighboring sites, but the height g_x of the current growth site depends on the current configuration. Hence the $m = \infty$ limit of model II is represented by the following two rules:

(i) For each generation, choose at random a permutation π of the numbers $1, \ldots, L$.

(ii) Update the height at each site x according to (1.1), in the order given by π, using each time the current height configuration on the right-hand side of (1.1).

Consequently, L particles are deposited in each generation, i.e., $J=1$ in Eq. (2.2). Numerically we find that the surface roughens at arbitrarily small tilt $u > 0$, and the growth velocity $v(u) > 1$ for $u > 0$ with a break in slope at $u = 0$. For $u > 0$, $v(u)$ is a smooth function of u. Using the technique described in Ref. 10, $v(u)$ can be computed for a strip of width $L = 2$ with periodic boundary conditions. The result is

$$v(u) = \begin{cases} 1 + u/2, & u \leq 1/2 \\ \tfrac{1}{2} + 3u/2, & u > 1/2 . \end{cases} \tag{4.2}$$

Apart from the break in slope at $u = \tfrac{1}{2}$, which is an artifact of the approximation, this result reproduces the main qualitative features of the large-system limit, i.e., the porosity $[\rho(u) = 1/v(u) < 1]$ for arbitrarily small u, the large asymptotic growth angle $\psi_0 = \arctan 3 \simeq 71.6°$ [cf. Eq. (2.6)], and the fact that the transverse growth velocity is *larger* than unity, $v_\perp = \tfrac{3}{2}$ [cf. Eq. (2.5)]. Numerically we find $v_\perp \simeq 1.70$ and $\psi_0 \simeq 67°$ for a strip of width $L = 1000$.

For model I it may happen, for a tilted substrate, that a growth site (x, g_x) is shadowed by a deposition event at $x+1$ or $x-1$ before its associated counter reaches maturity. At that point the counter associated with the newly created growth site at $g_x' > g_x$ is activated. However, the new counter belongs to the next generation, and hence in the current generation no growth takes place above the substrate site x. This implies that only a (u-dependent) fraction of the L growth sites is filled in each generation. Accordingly, for model I the rule (ii) formulated above for model II is modified into the following:

(ii') Select the substrate sites in the order given by π. For each site x check if the height of the growth site g_x

has changed as a result of previous depositions within the current generation. If not, fill it; otherwise, move on to the next growth site without filling the site at x.

Inspection of this rule for substrate inclinations $u \leq 1$ shows a *layerwise* displacement of the growth sites $g_x(n+1)=g_x(n)+1$ for the nth generation, despite the porosity due to shadowing. In other words, the particle current J and the deposit density ρ in (2.2) adjust such that $v(u)=J(u)/\rho(u)=1$ for all $u \leq 1$. The function $\rho(u)$ is computed below.

To analyze the behavior for $u > 1$ we turn to the growth of a fan from a point seed at $x=0$ under the rules (i) and (ii'). It is easily seen that the growth sites associated with the fan at generation n form a regular "hat" shape (Fig. 13)

$$g_x(n)=n-|x|, \quad -x_-(n) \leq x \leq x_+(n) , \qquad (4.3)$$

where, however, the edge positions x_- and x_+ are random. Clearly the fan grows sideways only if the leftmost or rightmost growth site is filled. This occurs with some probability which we identify as the lateral growth velocity $v_\perp$, i.e., $\langle x_+(n) \rangle \approx \langle x_-(n) \rangle \approx v_\perp n$ for large n. Hence the scaled shape function for the fan is given by [cf. Eq. (2.10)]

$$\mu(y)=1-|y|, \quad -v_\perp \leq y \leq v_\perp . \qquad (4.4)$$

Taking the inverse Legendre transform of (4.4) we obtain the inclination-dependent growth velocity

$$v(u)= \begin{cases} 1, & u \leq 1 \\ 1+v_\perp(u-1), & u > 1 . \end{cases} \qquad (4.5)$$

The lateral growth velocity $v_\perp$ is computed as follows.

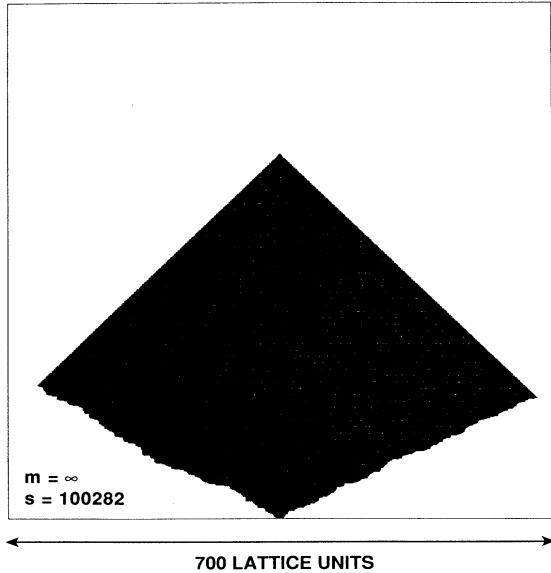m = ∞
s = 100282

◄———————— 700 LATTICE UNITS ————————►

FIG. 13. Cluster grown by ballistic deposition onto a point seed, using the $m = \infty$ limit of the noise reduced model I. The cluster contains 100 282 particles.

Let p_x denote the probability that the growth site at x is filled in a given generation n, $-x_-(n) \leq x \leq x_+(n)$. Clearly $p_x=p_{-x}$, so we focus on $x > 0$. We pick a permutation π of the numbers $0, \ldots, M=x_+(n)$ at random, such that the kth site to be selected is given by $\pi(x)=k-1$. Due to the simple structure (4.3) of the set of growth sites, the site at x can be shadowed only by a previous deposition at $x-1$. The top site $x=0$ cannot be shadowed. The site at $x=1$ is shadowed if $\pi(1)>\pi(0)$. This holds with probability $1-p_1=\frac{1}{2}$. The site at $x=2$ is certainly filled if $\pi(2)<\pi(1)$. A second possibility is that $\pi(2)>\pi(1)$, but that the site at $x=1$ was already shadowed when it was selected at $k=\pi(1)+1$, i.e., $\pi(2)>\pi(1)>\pi(0)$. The probability for this event is $1/3!=\frac{1}{6}$, hence $p_2=\frac{1}{2}+\frac{1}{6}=\frac{2}{3}$. To compute p_3 we must evaluate the joint probability that $\pi(3)>\pi(2)$ *and* the site at $x=2$ is not filled. This implies that $\pi(3)>\pi(2)>\pi(1)$ *and* the site at $x=1$ is filled, i.e., $\pi(1)<\pi(0)$. Thus the four numbers $\pi(0), \ldots, \pi(3) \in \{0,\ldots,M\}$ are to be arranged such that either $\pi(0)>\pi(3)>\pi(2)>\pi(1)$ or $\pi(3)>\pi(0)>\pi(2)>\pi(1)$ or $\pi(3)>\pi(2)>\pi(0)>\pi(1)$. Each possibility has a weight $1/4!$, hence the joint probability is $3/4!$ and $p_3=\frac{1}{2}+3/4!=\frac{5}{8}$. Proceeding inductively in this fashion it can be shown that

$$p_x= \begin{cases} \displaystyle\sum_{j=1}^{(x+1)/2} \frac{2j-1}{(2j)!} & \text{for } x \text{ odd} \\[2ex] p_{x-1}+\dfrac{1}{(x+1)!} & \text{for } x \text{ even} . \end{cases} \qquad (4.6)$$

The lateral growth velocity is the occupation probability for the outermost growth site at $x_+(n)$ in the macroscopic limit $n \to \infty$,

$$v_\perp= \lim_{x \to \infty} p_x=1-e^{-1} \simeq 0.632\,1205. \ldots \qquad (4.7)$$

This corresponds to a growth angle $\psi_0=\arctan(e-1)$ $\simeq 59.8°$ [cf. Eqs. (4.5), (2.5), and (2.6)]. We have also determined $v_\perp$ numerically. From a small-scale ($L=150$) measurement of the growth velocity $v(u)$ we obtain $v_\perp=0.630\pm0.005$, while the direct evaluation of fan shapes such as that shown in Fig. 13 yields $v_\perp=0.637\pm0.011$, both in good agreement with (4.7).

We noted above that the deposit density $\rho(u)$ for $u \leq 1$ is equal to the fraction $J(u)$ of growth sites which are occupied in each generation. $J(u)$ is easily obtained from the probabilities (4.6). Consider first inclinations

$$u_l=l/(l+1), \quad l=0,1,2,\ldots . \qquad (4.8)$$

The set of growth sites decomposes into sequences of length $l+1$, such that l sites sit next to a step $(g_{x+1}-g_x=1)$ and the (rightmost) $(l+1)$th site sits on the edge of a "terrace" $(g_{x+1}=g_x)$ of width 2. The terrace site cannot be shadowed, whereas each step site can be shadowed by deposition onto the site to the right of it. Hence the occupation probability for the kth site to the left of the terrace site is p_k. This implies a lateral variation of the deposit density, with wavelength $l+1$ and high-density $(\rho=1)$ streaks below the terrace sites. The
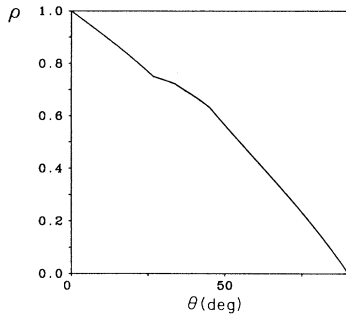
FIG. 14. Exact angular dependence of the deposit density for the $m = \infty$ limit of the noise-reduced model I.

overall occupation fraction is obtained by averaging over one sequence,

$$\rho(u_l)=J(u_l)=\frac{1}{l+1}\sum_{k=0}^{l}p_k \ . \tag{4.9}$$

At intermediate inclinations the density can be shown to interpolate linearly in u. For $u>1$ the exposed parts of the surface are facets of unit slope. Therefore $J(u)$ remains constant at $J(1)=v_{\perp}$ and $\rho(u)=v_{\perp}/v(u)$. The resulting dependence of the deposit density on the angle of incidence $\theta=\arctan u$ is depicted in Fig. 14.

For $u>1$ we expect the same kind of ideal columnar growth as in the faceted phase of the finite-density model (1.4): The growth velocity (4.5) is strictly linear in u, and the cusp at $u=1$ leads to faceted tips (Fig. 15). Numerical measurements of the surface roughness $\xi(t)$ support
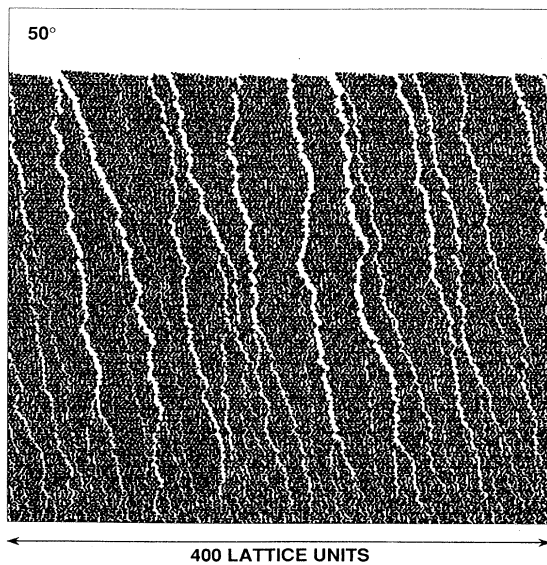
this picture; i.e., we find $\xi(t)\sim t^{1/2}$ at long times for all $u>1$. The random-walk arguments presented in Sec. III B to describe the crossover in $\xi(t)$ close to $u=1$ carry over without alteration (see Fig. 15 for a visualization of the diffusing facet boundaries), and the scaling form (3.20) is well supported by the simulations (Fig. 16). The main difference is that the flat phase, which was previously confined to $\theta=45°$, now extends to all $\theta\le 45°$, with a novel kind of "tilt-induced" roughening transition occurring at $\theta=45°$. We also note that in the present model, faceted growth at $\theta=45°$ is sustained at an occupation density $(v_{\perp})$ which is *below* the directed percolation threshold $p_c=0.705\,489$. Clearly this is possible because rule (ii') leads to a highly correlated occupation process, e.g., vacancies are never created at neighboring sites.

Summarizing, we conclude that for model I the limit $m\to\infty$ selectively suppresses fluctuations which lead to kinetic roughening at small angles of incidence $(\theta<45°)$, while those fluctuations which are necessary for column formation and competition survive even at $m=\infty$. This clearly demonstrates that the two types of fluctuations can be distinguished. In the original model (1.1), as well as in the $m=\infty$ limit of model II, both types are present simultaneously. Presumably this is the reason for the

FIG. 15. Deposit generated using the $m=\infty$ limit of model I for noise-reduced ballistic deposition. The angle of incidence is $\theta=50°$.
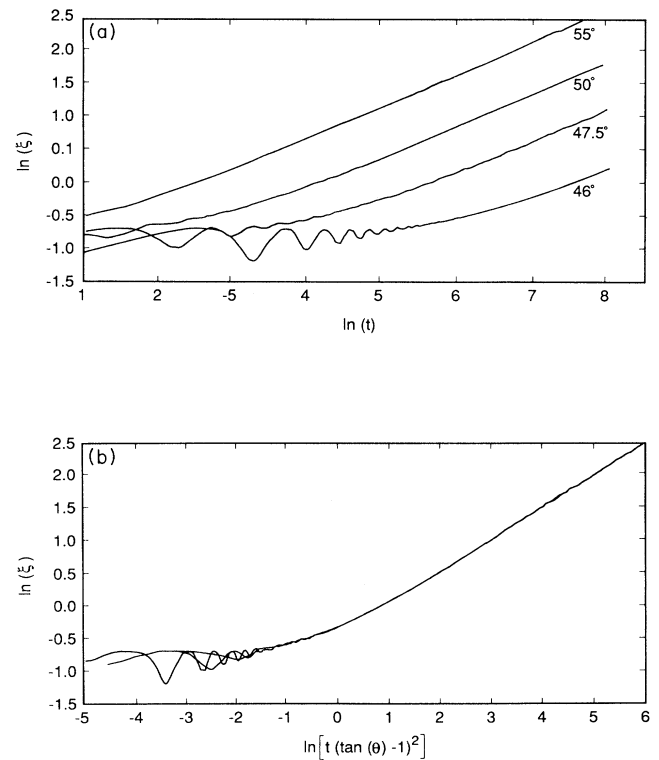
FIG. 16. Numerical confirmation of the scaling form (3.20) for the $m=\infty$ limit of model I for noise-reduced ballistic deposition at angles of incidence near 45°. (a) shows $\xi(t)$ at four angles, (b) shows the same data scaled according to (3.20).

complicated scaling behavior observed[10,13] at intermediate angles of incidence.

V. MEAN-FIELD THEORY

The mean-field approach to growth processes[28,31,51] is based on the—rather drastic—assumption that growth probabilities at neighboring lattice sites are independent. Such an approximation cannot account for statistical scaling properties, but it is a useful tool for studying macroscopic features such as growth shapes[28] and morphological transitions.[28,51] Moreover, there is some indication[28] that the mean-field theory becomes exact in the limit of infinite spatial dimensionality. In this section we explore in some detail an extension of the mean-field theory for ballistic deposition[52] originally proposed by Bensimon, Shraiman, and Kadanoff.[31]

A. Basic equations and density profiles

We work on a d-dimensional hypercubic lattice. Particles move in the negative y direction and the $d-1$ transverse coordinates are denoted by $\mathbf{x}$. We wish to derive the mean-field equations for the d-dimensional generalization of the finite-density deposition model (1.4). Let $\tilde{\rho}_t(\mathbf{x},y)$ be the probability for site $(\mathbf{x},y)$ to be part of the deposit at time t. Growth occurs with probability p at a site $(\mathbf{x},y)$ if

(i) *the site is a growth site:* it is vacant and either site $(\mathbf{x},y-1)$ or at least one of the $2(d-1)$ transverse neighbors $(\mathbf{x}+\mathbf{e},y)$, where $\mathbf{e}$ is a transverse lattice vector, belongs to the deposit; and

(ii) *the site is not shadowed:* all sites $(\mathbf{x},y')$ and $(\mathbf{x}+\mathbf{e},y')$ with $y'>y$ are vacant. Within the mean-field approximation this leads to the evolution equation

$$\tilde{\rho}_{t+1}(\mathbf{x},y)-\tilde{\rho}_t(\mathbf{x},y)=p\left\{1-[1-\tilde{\rho}_t(\mathbf{x},y-1)]\prod_{\mathbf{e}}[1-\tilde{\rho}_t(\mathbf{x}+\mathbf{e},y)]\right\}\prod_{y'=y}^{\infty}\left\{[1-\tilde{\rho}_t(\mathbf{x},y')]\prod_{\mathbf{e}}[1-\tilde{\rho}_t(\mathbf{x}+\mathbf{e},y'+1)]\right\} \quad (5.1)$$

The infinite product on the right-hand side clearly reflects the nonlocal nature of the deposition process. In the limit $p\to0$ combined with a rescaling of time (5.1) reduces to the continuous-time equation written down by Bensimon *et al.*[31]

We are interested in initial conditions corresponding to a substrate with inclination $u=\tan\theta$, which we choose as

$$\tilde{\rho}_0(\mathbf{x},y)=\begin{cases}1, & y<ux_1\\0, & y>ux_1 .\end{cases} \quad (5.2)$$

The homogeneity of the density in the remaining $d-2$ transverse directions $x_2,\ldots,x_{d-1}$ is preserved under (5.1). Hence the solution can be expressed in terms of a *one-dimensional* density profile,

$$\tilde{\rho}_t(\mathbf{x},y)=\rho_t(y-ux_1) , \quad (5.3)$$

which satisfies

$$\rho_{t+1}(z)-\rho_t(z)=p[1-\rho_t(z)]\{1-[1-\rho_t(z-1)][1-\rho_t(z-u)][1-\rho_t(z+u)][1-\rho_t(z)]^{2d-4}\}$$
$$\times\prod_{z'=z+1}^{\infty}[1-\rho_t(z')]^{2d-3}[1-\rho_t(z'-u)][1-\rho_t(z'+u)] , \quad (5.4)$$

with $z=y-ux_1$. In the following we consider only integer values of u, so Eq. (5.4) operates on the lattice of integers.

In Fig. 17 we show some examples of density profiles generated by (5.4). Note first that (5.4) is exact in the deterministic limit $p=1$: For $u\leq1$, the initial profile is simply shifted at unit velocity, while for $u>1$ a periodic density profile builds up,

$$\rho_t(z)=\begin{cases}1, & z=nu, \quad n=1,\ldots,t\\0, & \text{otherwise}\end{cases} \quad (5.5)$$

as a result of the growth of "needles" perpendicular to the y axis.[10] For $p<1$ the density oscillations are damped, with a decay time which diverges in both the limits $p\to1$ and $u\to\infty$ (cf. Fig. 17). The oscillations reflect, in an average way, the initial stages of columnar growth: Columns originate at the edges of the substrate steps. Moving up the y axis, a periodic sequence of high-

and low-density regions is encountered, the nth density maximum corresponding to a column which originated from a step n lattice constants away in the positive x_1 direction. This implies that the spacing Δ of the maxima is related to the columnar growth angle ψ through

$$\Delta=u+\cot\psi . \quad (5.6)$$

For long times, columns originating at different substrate sites lose their phase coherence, and the density oscillations are washed out and eventually vanish. To demonstrate this effect for the full stochastic model (1.1), Fig. 18 shows density profiles obtained from a square-lattice simulation by laterally averaging the density at sites (x,y) with $y-ux=z$. This yields the appropriate quantity for comparison with the mean-field profile (5.3). The decay of the density oscillations is much more rapid in the stochastic case, as would be expected.

Despite the simplifications of the mean-field approxi-

mation, solving the full nonlinear difference equation (5.4) still poses a formidable task. Fortunately, only the *linearized* dynamics is needed[28,29] to extract the basic quantity of interest, the inclination-dependent growth velocity. We first note that asymptotically (at times large enough for the density oscillations to have decayed) the solution to (5.4) can be written as a traveling wave, $\rho_t(z) = f(z - ct)$, where c is the growth velocity we wish to determine and f satisfies the boundary conditions $f(x \to -\infty) = 1$, $f(x \to \infty) = 0$. In the tail of the profile, we expect an exponential decay as

FIG. 18. Laterally averaged density profile obtained from a square-lattice simulation on a strip of width $L = 1000$, an angle of incidence of $\theta = 84.3°$, and a deposition flux of $p = 0.9$.

$$\rho_t(z) \sim e^{-q(z - ct)} \tag{5.7}$$

for some $q > 0$. Inserting this ansatz into (5.4) and linearizing the right-hand side we obtain a dispersion relation between c and q,

$$c(q) = \frac{1}{q}\ln\{1 + p[e^q + 2\cosh(qu) + 2d - 4]\} . \tag{5.8}$$

Quite surprisingly, the ansatz (5.7) does not fix the front velocity. There exist traveling wave solutions for any $c > c^*$, where c^* is the minimal value of (5.8). For a large class of partial differential[29,53] and difference[54] equations similar to (5.4) it can be shown that the actual front velocity is determined by the asymptotic decay of the initial condition $\rho_0(z)$ at large z. Localized initial conditions, such as the step profile (5.2), travel at the *minimal* speed c^*. Hence the inclination-dependent growth velocity $v(u)$ is obtained by minimizing (5.8) relative to q,

$$v(u) = c^* = \min_{q > 0} c(q) . \tag{5.9}$$

Clearly from now on the inclination u can be regarded as a continuous variable.

Before turning to the evaluation of (5.9) in specific cases of interest, we demonstrate the validity of the above analysis by comparing the predictions of the variational formula (5.9) to the direct numerical iteration of the difference equation (5.4). This check is important, since the selection of the minimal speed is known to break down[30] for certain mean-field growth models.[55]

The theory leading to (5.9) also predicts[30] that the front velocity converges to its asymptotic value c^* from below, with a leading correction term[39] proportional to $1/t$. Using the general relation (2.2) with $J = p$, this result implies a $1/z$-decay of the frozen density profile,

$$\rho_t(z) \approx \rho_0 + A/z, \quad 1 \ll z \ll ct , \tag{5.10}$$

with $\rho_0 = p/c^*$ and[30]
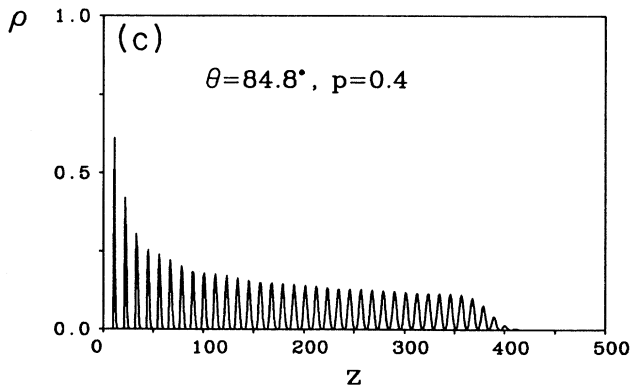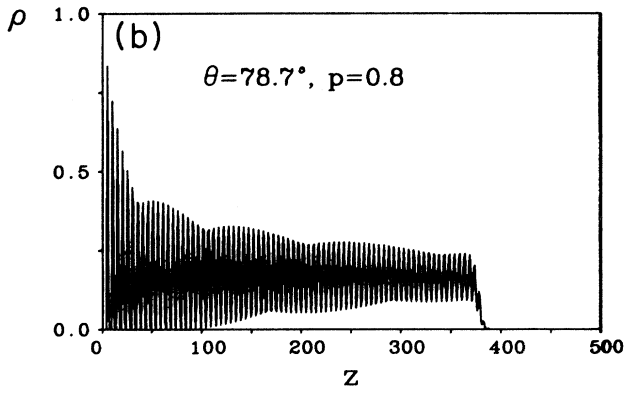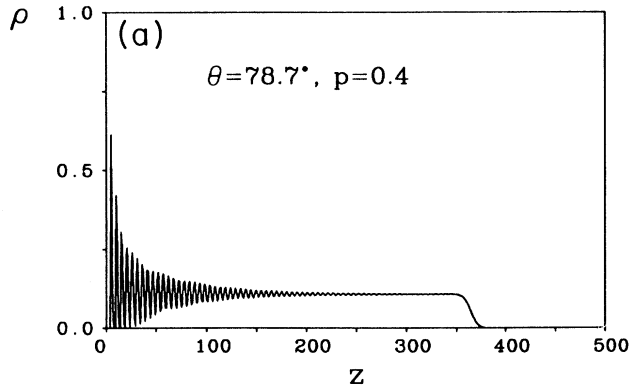
$$A = \frac{3\rho_0}{2q^*} . \tag{5.11}$$

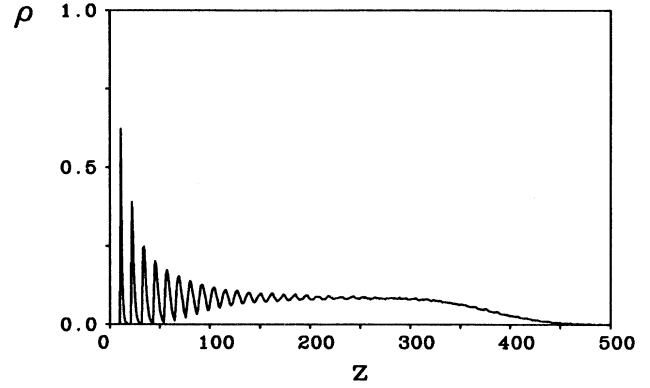FIG. 17. Density profiles $\rho_t(z)$ generated by the mean-field equation (5.4).
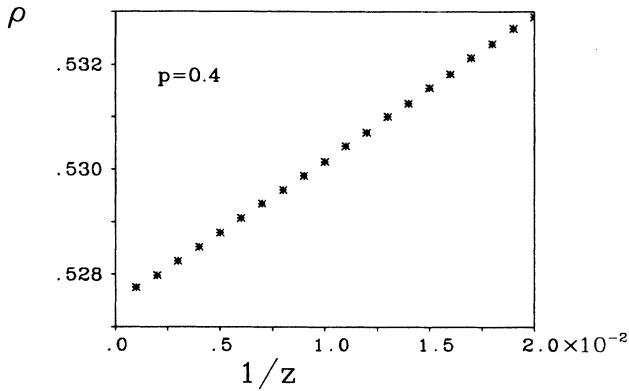
FIG. 19. Mean-field density profile $\rho_t(z)$ obtained by iterating the difference equation (5.4) up to $t=5000$, with $p=0.4$. The convergence to the asymptotic density is linear in $1/z$.

Here q^* denotes the value of q at which the minimum in (5.9) is attained.

We have iterated (5.4) for normal-incidence deposition ($u=0$) at various values of p, and analyzed the frozen density profile up to $z=1000$. Figure 19 confirms the expected asymptotic $1/z$ decay, and Table I compares the results for ρ_0 and A, obtained from a least-squares fit of the density profile to (5.10), to the predicted values. The agreement is excellent for ρ_0, and the correction amplitude A is proportional to ρ_0/q^* as predicted. However, the coefficient of proportionality turns out to be 1.384 ± 0.007 rather than the simple fraction $\frac{3}{2}$ in (5.11).

B. The phase diagram

The mean-field theory of faceting and directed percolation has been presented in detail elsewhere.[28] Here we briefly review the main results of interest in the present context. As the mean-field critical behavior is independent of dimension, we restrict ourselves to $d=2$.

It was pointed out in Sec. III that the emergence of faceted growth at $u=1$ is related to an asymptotically finite density $\sigma(t)$ of occupied sites on the line $y-x_1=t$.

TABLE I. Asymptotic deposit density ρ_0 and amplitude A of the leading $1/z$ correction for the mean-field theory of ballistic deposition. We compare the asymptotic density $\rho_0^{(1)}$ obtained by iterating the difference equation (5.4) to the prediction $\rho_0^{(2)}$ of the variational formula (5.9). The last column shows that A is proportional to ρ_0/q^*, cf. Eq. (5.11).

p	$\rho_0^{(1)}$	$\rho_0^{(2)}$	A	q^*A/ρ_0
0.1	0.304 858	0.304 865	0.240	1.391
0.2	0.378 593	0.378 575	0.253	1.379
0.3	0.452 722	0.452 726	0.267	1.385
0.4	0.527 429	0.527 423	0.275	1.381
0.5	0.602 807	0.602 799	0.280	1.380
0.6	0.678 981	0.679 017	0.285	1.395
0.7	0.756 306	0.756 294	0.277	1.374

Within the mean-field approximation, $\sigma(t)=\rho_t(t)$. From (5.4) we infer the autonomous time evolution[51]

$$\sigma(t+1)=p(1-[1-\sigma(t)]^2) .\qquad (5.12)$$

For $p<p_c=\frac{1}{2}$ the fixed point $\sigma=0$ is stable, $\sigma(t)=(2p)^t\sigma(0)\sim e^{-t/\xi_t}$ with $\xi_t=-1/\ln(2p)$. Thus the mean-field value[18] of the correlation length exponent v_t [cf. Eq. (3.4)] is $v_t=1$. For $p>p_c$ a nontrivial fixed point $\sigma_0\sim p-p_c$ appears, leading to the value $\beta_{DP}=1$ for the order-parameter exponent[18] [Eq. (3.5)]. A detailed analysis[28] of the inclination-dependent growth velocity (5.9) shows that a break in slope at $u=1$ appears for $p>p_c$, with a magnitude proportional to $(p-p_c)^{1/2}$. Comparison with (3.12) then implies that $v_r=\frac{1}{2}$ in the mean-field approximation. Similarly, the growth-shape singularities discussed in Sec. III A can be computed[28] and shown to be consistent with the general scaling theory[21] in the limit $d\to\infty$.

Since the solutions to (5.4) are of the traveling-wave form (5.7), the width of the surface is asymptotically finite, and kinetic roughening does not occur. A distinction between "rough" and "flat" growth morphologies can still be made using the inverse of the decay constant q in (5.7) as a measure of the surface roughness ξ. Asymptotically, the selected value of q is the position q^* of the minimum of (5.8), hence we write

$$\xi=1/q^* .\qquad (5.13)$$

For $u=1$ and $p>p_c=\frac{1}{2}$ we have seen that $\rho_t(t)=\sigma_0>0$ for $t\to\infty$. On the other hand, it is an immediate consequence of (5.4) that $\rho_t(z)\equiv0$ for $z>t$. Thus for $u=1$ and $p>p_c$ the profile is *discontinuous* at $z=t$ and the exponential tail in (5.7) does not exist. Within our mean-field theory, faceting is therefore related to the divergence of q^*, i.e., the vanishing of ξ, on approaching the line $u=1$, $p>p_c$. This becomes evident by expanding (5.8) for large q. We obtain

$$c(q)\approx\begin{cases}1+q^{-1}\ln(p), & u<1\\1+q^{-1}\ln(2p), & u=1\\u+q^{-1}\ln(p), & u>1 .\end{cases}\qquad (5.14)$$

For $u<1$ and $u>1$ the asymptotic ($q\to\infty$) value of c is approached from below, hence a finite minimum $q^*<\infty$ must exist. For $u=1$ this is true only for $p<p_c=\frac{1}{2}$. A more careful analysis[28] yields the following critical behavior of ξ:

$$\xi\sim\begin{cases}-1/\ln(p_c-p), & u=1, \quad p\to p_c^-\\|u-1|, & p>p_c, \quad u\to1 .\end{cases}\qquad (5.15)$$

It might seem reasonable to conclude that the mean-field phase diagram is quite similar to that of the full stochastic model (Sec. III): For $p>p_c$ there is a flat phase ($\xi=0$) at $u=1$, sandwiched between two rough phases ($\xi>0$) for $u<1$ and $u>1$. However, there is an important dissimilarity regarding the symmetry of the phase diagram with respect to $u=1$. For the stochastic model we showed that the two rough phases, the continuous

growth phase ($u < 1$) and the columnar growth phase ($u > 1$), are very different with regard to both macroscopic properties and scaling behavior. In contrast, the mean-field approximation gives rather similar results on both sides of $u = 1$. As an example, Fig. 20 shows the columnar-growth angle $\psi(\theta)$ calculated from the mean-field growth velocity (5.9) and the general formula (2.4). For $p > p_c$ the growth angle is discontinuous, corresponding to the cusp in $v(u)$. However, for $\theta > 45°$ $\psi(\theta)$ is not constant, as would be expected for columnar growth (cf. Fig. 5). In fact, the figure looks rather symmetric with respect to $\theta = 45°$. A similar conclusion can be drawn in the case $p = 0$, where it is seen [Fig. 20(b)] that $\psi(\theta)$ reaches its grazing incidence value ψ_0 at a finite slope, rather than showing a plateau[13] for large θ. In terms of the theory of Sec. II this indicates that the correction exponent in Eq. (2.7) is $n = 1$ for the mean-field approxima-

FIG. 20. Column orientation ψ as a function of the angle of incidence θ computed in the mean-field approximation. (a) $p = 0.6$, (b) $p = 0$.

tion, as will be explicitly shown below. These observations can be summed up in the statement that columnar growth cannot be accounted for by the mean-field theory, the reason being that some amount of noise is needed to initiate and maintain the competitive columnar-growth process.

Before turning to the high-dimensionality behavior we briefly comment on a striking feature of Fig. 20(a), viz. the flatness of the function $\psi(\theta)$ close to the discontinuity at $\theta = 45°$. It follows from the general expression (2.4) that this regime is related to the cluster shape close to the facet, equivalently to the next to leading term in $v(u)$ close to the cusp at $u = 1$ [cf. Eq. (2.15)]. In d dimensions the next to leading term can be shown[21] to be proportional to $(1 - u)^{1/\beta_d - 1}$ for $u < 1$, where β_d is the kinetic roughening exponent for a continuous $(d - 1)$-dimensional surface, $\beta_1 = \frac{1}{2}$, and $\beta_2 = \frac{1}{3}$, cf. Sec. III B. The growth angle then approaches the discontinuity as $\psi_- - \psi(u) \sim |u - 1|^{1/\beta_d - 1^{-1}}$, where $\psi_- = \lim_{u \to 1-0} \psi(u)$. We noted above that $\beta = 0$ in the mean-field theory, and therefore the next to leading term in $v(u)$ is exponential in $1/(1 - u)$.[28] This implies an essential singularity in $\psi(u)$ as well,

$$|\psi(u) - \psi_\pm| \sim |u - 1|^{-1} e^{-a/|u - 1|} , \qquad (5.16)$$

where $\psi_\pm = \lim_{u \to 1\pm0} \psi(u)$ and $a = a(p) > 0$.

C. High-dimensionality behavior

Experience from equilibrium statistical mechanics leads us to expect that an approximation of mean-field type would become more accurate in high spatial dimensionality. For example, it has been shown[28] that the mean-field approach reproduces the exact large d asymptotics[56] for the growth velocity of the Eden model.[57] Here we present a comparison of the mean-field predictions with simulation results for the dimensionality dependence of two basic macroscopic quantities in ballistic deposition, the deposit density at normal particle incidence and the opening angle of clusters grown from a seed (cf. Sec. II).

For simplicity we discuss only the sequential lattice model (1.1), corresponding to the dilute limit $p \to 0$ of model (1.4) in d spatial dimensions. In the limit $p \to 0$, combined with a rescaling $c \to c/p$, the dispersion relation (5.8) becomes

$$c(q) = \frac{1}{q}[e^q + 2\cosh(qu) + 2d - 4] , \qquad (5.17)$$

which must be minimized relative to q [cf. Eq. (5.9)]. Setting $u = 0$ in (5.17) and taking the derivative with respect to q we find that the deposit density at normal incidence, $\rho = 1/v(0)$, satisfies

$$\ln\rho + (2d - 2)\rho + 1 = 0 . \qquad (5.18)$$

For large d the solution behaves as

$$\rho(d) \approx \frac{\ln(2d - 1)}{2d - 1}\left[1 - \frac{\ln[\ln(2d - 1)]}{\ln(2d - 1)} + O(1/\ln d)\right] . \qquad (5.19)$$
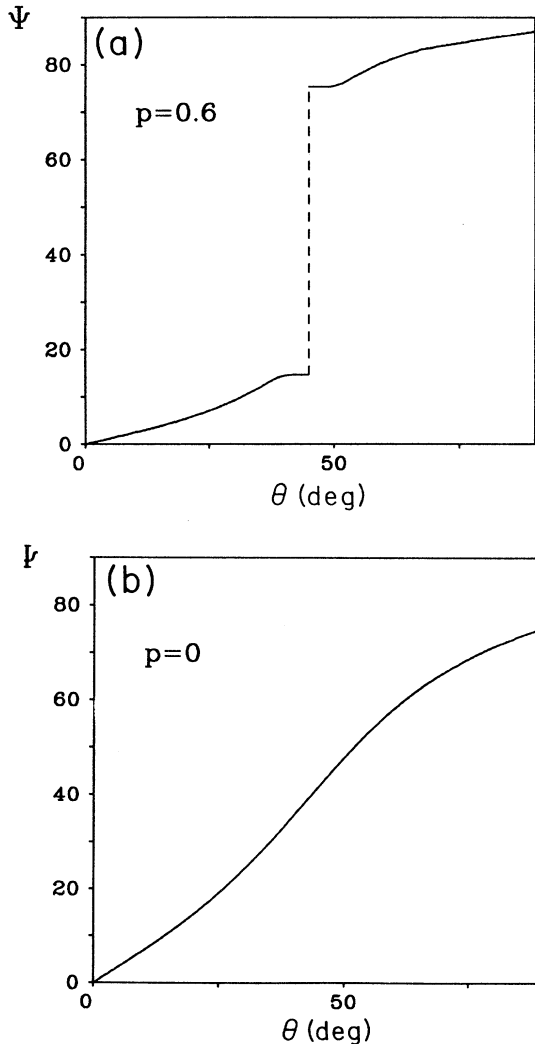
The porosity increases in high dimensions. In Table II we compare the solution of (5.18) to numerical results obtained from large-scale simulations in dimensions $d = 2-6$. We used lattices of various transverse sizes L up to $L=2048$ $(d=2)$, $L=1024$ $(d=3)$, $L=128$ $(d=4)$, $L=32$ $(d=5)$, and $L=16$ $(d=6)$. For each value of L, deposits containing up to 6×10^9 particles were generated. The results were extrapolated to $L = \infty$ using the finite-size scaling relation[39]

$$\rho(L) - \rho(\infty) \sim L^{-\alpha_\parallel} , \qquad (5.20)$$

where the universal scaling exponent $\alpha_\parallel$ can be related[39] to the kinetic roughening exponent β [cf. Eq. (3.19)],

$$\alpha_\parallel = \frac{2(1-\beta)}{1+\beta} . \qquad (5.21)$$

In $d=2$, $\alpha_\parallel = 1$ exactly. Numerical estimates for β in dimensions $d = 3-6$ have recently been presented by Renz.[58] The resulting data for $\rho(\infty)$ shown in Table II demonstrate that the mean-field approximation strongly underestimates the deposit density. However, the predicted decrease of the density for increasing dimensionality is confirmed by the simulations and the density appears to slowly converge toward the mean-field prediction in the limit $d \to \infty$.

As explained in Sec. II, the opening angle ψ_0 of clusters grown from a seed can be computed from the asymptotics of the inclination-dependent growth velocity $v(u)$ for $u \to \infty$. Finding the minimum of (5.17) simplifies for large u by noting that the position q^* of the minimum moves to infinity as

$$q^* = \lambda/u , \qquad (5.22)$$

where λ is the solution of

$$\lambda \sinh\lambda - \cosh\lambda = d - \tfrac{3}{2} . \qquad (5.23)$$

The asymptotic behavior of the growth velocity is then given by

$$v(u) \approx 2u \sinh\lambda + 1 + \lambda/2u + O(1/u^2) . \qquad (5.24)$$

This shows that $n=1$ in the expansion (2.7) and leads to the identification [cf. Eq. (2.5)]

$$v_\perp = 2 \sinh\lambda \qquad (5.25)$$

and [cf. Eq. (2.6)]

$$v_\perp \cot\psi_0 = 1 . \qquad (5.26)$$

Inserting (5.25) into (5.23) one obtains the large-d asymptotic behavior

$$v_\perp \approx \frac{2d}{\ln d} , \qquad (5.27)$$

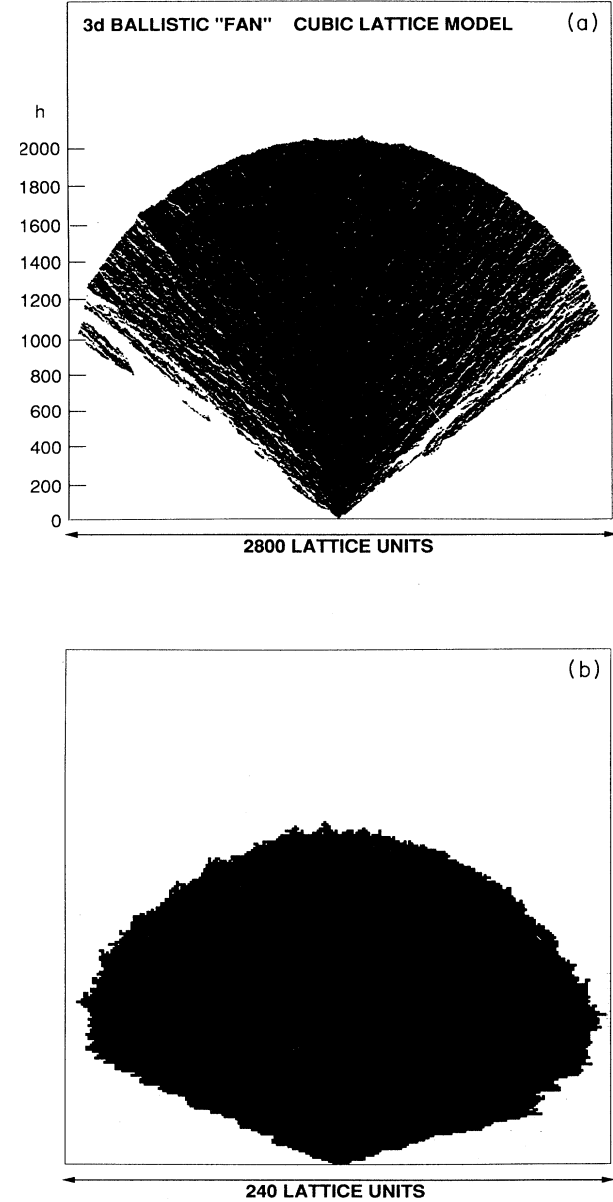and accordingly $\psi_0 \to 90°$ for $d \to \infty$. We note that (5.27)

FIG. 21. Clusters grown by deposition onto a point seed using the sequential ballistic deposition model on d-dimensional hypercubic lattices. (a) Cut through a three-dimensional cluster. (b) Projection of a four-dimensional cluster onto a plane which contains the direction of particle incidence.

TABLE II. Deposit density ρ extrapolated to the infinite-system limit and mean field prediction ρ^{MF} for normal-incidence ballistic deposition on d-dimensional hypercubic lattices.

d	ρ	ρ_{MF}	ρ/ρ_{MF}
2	0.4673	0.231 52	2.018
3	0.3000	0.179 45	1.672
4	0.2224	0.149 77	1.485
5	0.1784	0.130 01	1.372
6	0.1506	0.115 68	1.302

is the exact[56] asymptotics for the growth velocity of the Eden model.[57] This is not surprising, since transverse growth in d-dimensional ballistic deposition can be described by a $d-1$-dimensional Eden growth process.[11]

In two and three dimensions, the mean-field theory grossly overestimates the growth angle ψ_0, $\psi_0(d=2)=75.2°$ and $\psi_0(d=3)=78.9°$, as compared to the simulation results[10,11,13,32] $\psi_0(d=2)\simeq32.0°$ and $\psi_0(d=3)\simeq50°$. To check the predicted increase of ψ_0 with increasing dimensionality we have grown clusters on three- and four-dimensional lattices, which are displayed in Fig. 21.

Note added in proof. In the infinite noise reduction limit model I discussed in Sec. IV becomes equivalent to a one-dimensional random sequential filling problem with one-sided blocking. Our result (4.7) for the asymptotic filling fraction has been previously derived by González, Hemmer, and Høye.[59] We thank V. Privman for bringing this class of problems to our attention.

*Present address: IBM Thomas J. Watson Research Center, P.O. Box 218, Yorktown Heights, New York 10598.

[1]*Random Fluctuations and Pattern Growth,* Vol. 157 of *NATO Advanced Study Institute, Series E: Applied Sciences,* edited by H. E. Stanley and N. Ostrowsky (Kluwer, Dordrecht, 1988).

[2]H. Chou and H. Z. Cummins, Phys. Rev. Lett. **61**, 173 (1988); X. W. Qian, H. Chou, M. Muschol, and H. Z. Cummins, Phys. Rev. B **39**, 2529 (1989).

[3]A. Dougherty, P. D. Kaplan, and J. P. Gollub, Phys. Rev. Lett. **58**, 1652 (1987); R. Pieters and J. S. Langer, *ibid.* **56**, 1948 (1986); X. W. Qian and H. Z. Cummins, *ibid.* **64**, 3038 (1990).

[4]S.-C. Huang and M. E. Glicksman, Acta Metall. **29**, 717 (1981); M. E. Glicksman and P. W. Voorhees, Metall. Trans. **15A**, 995 (1984).

[5]H. J. Leamy, G. H. Gilmer, and A. G. Dirks, in *Current Topics in Materials Science,* edited by E. Kaldis (North-Holland, Amsterdam 1980), Vol. 6.

[6]H. König and G. Helwig, Optik **6**, 111 (1950).

[7]R. P. U. Karunasiri, R. Bruinsma, and J. Rudnick, Phys. Rev. Lett. **62**, 788 (1989).

[8]S. Lichter and J. Chen, Phys. Rev. Lett. **56**, 1396 (1986).

[9]A. Mazor, D. J. Srolovitz, P. S. Hagan, and B. G. Bukiet, Phys. Rev. Lett. **60**, 424 (1988); D. J. Srolovitz, A. Mazor, and B. G. Bukiet, J. Vac. Sci. Technol. A **6**, 2371 (1988).

[10]J. Krug and P. Meakin, Phys. Rev. A **40**, 2064 (1989).

[11]P. Meakin and J. Krug, Europhys. Lett. **11**, 7 (1990); P. Meakin (unpublished).

[12]Z. Ràcz and T. Vicsek, Phys. Rev. Lett. **51**, 2382 (1983); P. Meakin, Phys. Rev. B **30**, 4207 (1984).

[13]P. Meakin, Phys. Rev. A **38**, 994 (1988).

[14]R. Baiod, D. Kessler, P. Ramanlal, L. Sander, and R. Savit, Phys. Rev A **38**, 3672 (1988); Z. Cheng, L. Jacobs, D. Kessler, and R. Savit, J. Phys. A **20**, L1095 (1987).

[15]F. Family and T. Vicsek, J. Phys. A **18**, L75 (1985).

[16]P. Meakin, P. Ramanlal, L. M. Sander, and R. C. Ball, Phys. Rev. A **34**, 5091 (1986).

[17]N. G. Nakhodkin and A. I. Shaldervan, Thin Solid Films **10**, 109 (1972); D. K. Pandya, A. C. Rastogi, and K. L. Chopra, J. Appl. Phys. **46**, 2966 (1975); K. H. Guenther, Appl. Opt. **23**, 3806 (1984); K.-H. Müller, J. Appl. Phys. **58**, 2573 (1985).

[18]W. Kinzel, Ann. Isr. Phys. Soc. **5**, 425 (1983); J. W. Essam, A. J. Guttmann and K. De'Bell, J. Phys. A **21**, 3815 (1988).

[19]D. Richardson, Proc. Cambridge Philos. Soc. **74**, 515 (1973); R. Durrett and T. M. Liggett, Ann. Prob. **9**, 186 (1981); R. Savit and R. Ziff, Phys. Rev. Lett. **55**, 2515 (1985).

[20]J. Kertész and D. E. Wolf, Phys. Rev. Lett. **62**, 2571 (1989); C. Lehner, N. Rajewsky, D. E. Wolf, and J. Kertész, Physica A **164**, 81 (1990).

[21]J. Krug, J. Kertész, and D. E. Wolf, Europhys. Lett. **12**, 113 (1990).

[22]G. H. Gilmer, M. H. Grabow, and A. F. Bakker, Mater. Sci. Eng. B **6**, 101 (1990).

[23]J. Szép, J. Cserti, and J. Kertész, J. Phys. A **18**, L413 (1985); C. Tang, Phys. Rev. A **31**, 1977 (1985); J. Kertész and T. Vicsek, J. Phys. A **19**, L257 (1986); P. Meakin, J. Kertész, and T. Vicsek, *ibid.* **21**, 1271 (1988); J.-P. Eckmann, P. Meakin, I. Procaccia, and R. Zeitak, Phys. Rev. A **39**, 3185 (1989); Phys. Rev. Lett. **65**, 52 (1990).

[24]P. Meakin, Phys. Rev. A **38**, 418 (1988).

[25]J. Kertész and D. E. Wolf, J. Phys. A **21**, 747 (1988); D. E. Wolf and J. Kertész, *ibid.* **20**, L257 (1987); Europhys. Lett. **4**, 651 (1987).

[26]P. Devillard and H. E. Stanley, Phys. Rev. A **38**, 6451 (1988); Physica A **160**, 298 (1989).

[27]J. Krug and H. Spohn, Phys. Rev. A **38**, 4271 (1988).

[28]J. Krug and H. Spohn, in *Solids Far From Equilibrium: Growth, Morphology and Defects,* edited by C. Godrèche (Cambridge University, Cambridge, England, 1991).

[29]W. van Saarloos, Phys. Rev. A **37**, 211 (1988).

[30]W. van Saarloos, Phys. Rev. A **39**, 6367 (1989).

[31]D. Bensimon, B. Shraiman, and L. P. Kadanoff, in *Kinetics of Aggregation and Gelation,* edited by F. Family and D. P. Landau (Elsevier, Amsterdam, 1984).

[32]D. Bensimon, B. Shraiman, and S. Liang, Phys. Lett. **102A**, 238 (1984); S. Liang and L. P. Kadanoff, Phys. Rev. A **31**, 2628 (1985); A. V. Limaye and R. E. Amritkar, *ibid.* **34**, 5085 (1986); P. S. Joag, A. V. Limaye, and R. E. Amritkar, *ibid.* **36**, 3395 (1987).

[33]P. Ramanlal and L. M. Sander, Phys. Rev. Lett. **54**, 1828 (1985).

[34]J. Krug, J. Phys. A **22**, L769 (1989).

[35]P. Meakin and R. Jullien, J. Phys. (Paris) **48**, 1651 (1987); R. Jullien and P. Meakin, Europhys. Lett. **4**, 1385 (1987).

[36]J. Krug and H. Spohn, Phys. Rev. Lett. **64**, 2332 (1990).

[37]J. M. Nieuwenhuizen and H. B. Haanstra, Philips' Technische Rundschau **27**, 177 (1966).

[38]A. A. Chernov, Kristallografiya **7**, 895 (1962) [Sov. Phys. Crystallogr. **7**, 728 (1963)]; D. E. Wolf, J. Phys. A **20**, 1251 (1987).

[39]J. Krug and P. Meakin, J. Phys. A **23**, L987 (1990).

[40]C. Rottman and M. Wortis, Phys. Rep. **103**, 59 (1984); A. F.

Andreev, Zh. Eksp. Teor. Fiz. **80**, 2042 (1981) [Sov. Phys. JETP **53**, 1063 (1982)].

[41]The numerical procedure used to determine the columnar growth angle is described in Ref. 13.

[42]M. Kardar, G. Parisi, and Y. C. Zhang, Phys. Rev. Lett. **56**, 889 (1986); E. Medina, T. Hwa, M. Kardar, and Y. C. Zhang, Phys. Rev. A **39**, 3053 (1989).

[43]For a different type of rough-to-rough transition in surface growth, see J. G. Amar and F. Family, Phys. Rev. Lett. **64**, 543 (1990), and Ref. 36.

[44]P. Meakin, J. Phys. A **20**, L1113 (1987).

[45]M. Matsushita and P. Meakin, Phys. Rev. A **37**, 3645 (1988).

[46]M. Plischke and Z. Ràcz, Phys. Rev. A **32**, 3825.

[47]H. Kondoh, M. Matsushita, and Y. Fukuda, J. Phys. Soc. Jpn. **56**, 1913 (1987); H. Takayasu, I. Nishikawa, and H. Tasaki, Phys. Rev. A **37**, 3110 (1988).

[48]E. Domany and W. Kinzel, Phys. Rev. Lett. **53**, 311 (1984).

[49]M. Bramson and D. Griffeath, Z. Wahrscheinlichkeitstheorie verw. Gebiete **53**, 183 (1980).

[50]L. Peliti, J. Phys. A **19**, L365 (1986); K. Kang and S. Redner, Phys. Rev. A **30**, 2833 (1984).

[51]Z. Cheng, R. Baiod, and R. Savit, Phys. Rev. A **35**, 313 (1987).

[52]J. Cook and B. Derrida have independently developed a mean-field theory for ballistic deposition starting from the updating rule (1.1).

[53]D. G. Aronson and H. F. Weinberger, Adv. Math. **30**, 33 (1978); M. Bramson, Mem. Am. Math. Soc. **285**, 1 (1983).

[54]M. Bramson (unpublished).

[55]H. Brandstetter, Diploma Thesis, University of Munich (unpublished).

[56]D. Dhar, Phys. Lett. A **130**, 308 (1988).

[57]M. Eden, in *Symposium on Information Theory in Biology*, edited by H. P. Yockey (Pergamon, New York, 1958).

[58]W. Renz (private communication).

[59]J. J. González, P. C. Hemmer, and J. S. Høye, Chem. Phys. **3**, 228 (1974).